High temperature steam oxidation of chromium-coated zirconium-based alloys: Kinetics and process

J.-C. Brachet, E. Rouesne, J. Ribis, T. Guilbert, S. Urvoy, G. Nony, C. Toffolon-Masclet, Matthieu Le Saux, N. Chaabane, H. Palancher, et al.

Paper submitted to Corrosion Science

Title: "High Temperature Steam Oxidation of Chromium-Coated Zirconium-Based Alloys: Kinetics and Process"

Authors: Jean-Christophe BRACHET[1(*)], Elodie ROUESNE[1], Joël RIBIS[1], Thomas GUILBERT[1], Stéphane URVOY[1], Guillaume NONY[1], Caroline TOFFOLON-MASCLET[1], Matthieu LE SAUX[1,2], Nihed CHAABANE[3], Hervé PALANCHER[4], Amandine DAVID[5], Jérémy BISCHOFF[6], Julien AUGEREAU[7], Edouard POUILLIER[8]

Affiliations:
[1] CEA, DEN, DMN, Service de Recherches Métallurgiques Appliquées (SRMA), Université Paris-Saclay, F-91191 Gif-sur-Yvette, France
[2] *Now at ENSTA Bretagne, UMR CNRS 6027, IRDL, F-29200, Brest, France*
[3] CEA, INSTN, Université Paris-Saclay, F-91191, Gif-sur-Yvette, France
[4] CEA, DEN, DEC, F-13108 Saint-Paul-lez-Durance, France
[5] Tescan-Analytics, ZAC St. Charles, 3ème Rue – n° 131, 13710 Fuveau, France
[6] Framatome, 10 rue Juliette Récamier, 69456 Lyon, Cedex 06, France
[7] Framatome, Route de Nantes, BP 3021, 44560 Paimboeuf, France
[8] EDF R&D, MMC Department, avenue des Renardières, 77818 Moret-Sur-Loing, France

(*) corresponding author: jean-christophe.brachet@cea.fr

ABSTRACT:

The oxidation of chromium-coated zirconium-based alloys is studied under steam at temperatures ranging from 800°C up to 1500°C and for oxidation times ranging from a few minutes up to a few hours. For oxidation temperatures up to 1300°C, the overall oxidation kinetics is nearly parabolic at the beginning of oxidation, when the Cr outer layer is protective. Finally, it significantly accelerates and hydrogen is absorbed during a short period. These steps correspond to different oxidation and diffusion mechanisms, involving: growth of outer chromia scale; Zr-Cr interdiffusion, inducing $Zr(Cr,Fe)_2$ intermetallic layer thickening then disappearance due to transformation into metallic chromium and zirconia; transport of oxygen through residual chromium (in particular along grain boundaries) and into the zirconium substrate, and finally growth of a sub-coating zirconia. The additional effect of the Zr-Cr eutectic reaction occurring when the oxidation temperature is increased beyond 1300°C is also studied and briefly discussed.

KEYWORDS: chromium coating; zirconium alloys; high temperature steam oxidation; enhanced accident tolerant nuclear fuel claddings

HIGHLIGHTS:

- Oxidation of Cr-coated Zr alloys is studied under steam up to 1500°C.
- Oxidation kinetics vary depending on the actual protectiveness of the Cr coating.
- Different underlying diffusion mechanisms are highlighted.
- Cr volatilization appears to be negligible.
- Effect of Zr-Cr eutectic beyond 1300°C is studied.

1. INTRODUCTION

Due to a good balance between resistance to corrosion, neutron transparency and mechanical properties, zirconium-based alloys have been used since the 1960s for nuclear fuel claddings in Light Water Reactors (LWRs). However, since the Fukushima-Daiichi nuclear plants accident in 2011, there is an increasing international effort to develop Enhanced Accident Tolerant Fuels (EATF) cladding materials [1]-[6]. One of the main objective of such development is to increase the resistance of the nuclear fuel cladding to oxidation under steam at High Temperature (HT), typical of hypothetical Design Basis Accidents (DBA) such as LOss of Coolant Accident (LOCA) situations. Indeed, improving the HT oxidation resistance of the cladding may induce several benefits upon LOCA transients, by:

- inducing additional "coping time" before embrittlement and failure of the cladding due to too severe oxidation;
- lowering the Peak Cladding Temperature (PCT) by reducing the contribution of the heat generated by the exothermic oxidation reaction of zirconium;
- decreasing the production of gaseous hydrogen and thus lowering the hydrogen explosion risk as experienced in some of the Fukushima-Daiichi nuclear plants.

Among the EATF concepts studied worldwide, metallic chromium-based coatings deposited by using a Physical Vapor Deposition (PVD) process have shown encouraging results during the early prospective studies engaged at CEA [7] and during the more recent investigations carried out on $M5_{Framatome}$ (Zr1Nb) alloy substrate [8]-[18]. For example, it has been shown that, compared to conventional uncoated cladding materials, the corrosion kinetics of the last generation of Cr-coated Zr-based materials is drastically reduced upon out-of-pile autoclave corrosion tests carried-out during several hundred days at 350°C in representative PWR primary water chemistry and pressure [12]. Moreover, a recent overview on the behavior of coated zirconium-based claddings upon normal in-reactor operating conditions and HT oxidation conditions was made in [19]. The authors conclude that among the various coating families considered for EATF application, metallic chromium-based coatings show one of the best compromise between resistance to corrosion during in-service operation and under LOCA conditions. Currently, several institutes are studying Cr-based coatings deposited with different alternative processes [20]-[32]. This confirms the increasing international interest in Cr-coated Zr-based alloys.

Indeed, as far as appropriate deposition process/parameters and optimized thicknesses are used, Cr-coated materials show significantly slower HT steam oxidation rate than the uncoated zirconium-based reference cladding materials. The Cr-coating is thus able to induce a significant additional "grace period" before oxidation at HT becomes too detrimental to the material mechanical integrity. For example, as developed and discussed in [18], for 12-15µm-thick Cr-coated Zr-based materials, the one-sided oxidation time at 1200°C, above which the cladding becomes brittle after low temperature quenching, is ten times higher than the ones of the uncoated reference claddings.

However, under steam and at temperatures up to at least 1300°C, the metallic Cr-coating is consumed by two simultaneous mechanisms: outer chromia formation and chromium diffusion into the β_{Zr} substrate. A preliminary model describing the kinetics of the overall consumption of the Cr-coating upon HT steam oxidation, typical of DBA and slightly beyond LOCA conditions, has been proposed in [7].

As an illustration of the specific HT oxidation behavior of Cr-coated Zr-based materials, Figure 1 shows the results of Thermogravimetric Analysis (TGA) measurements carried out in a helium-oxygen mixture at 1300°C on both uncoated and Cr-coated Zircaloy-4 sheet samples. It was checked that, for the HT oxidation temperature and time experienced here, the overall oxidation kinetics is nearly the same under helium-oxygen and under more LOCA-prototypical steam environments. One can observe the well-known parabolic oxidation kinetics of (uncoated) zirconium-based alloys. The weight gain evolution is more complex for the Cr-coated material. Indeed, the oxidation kinetics of the Cr-coated sample is nearly parabolic for oxidation times typical of DBA and slightly beyond conditions. For longer oxidation times, Cr loses its protectiveness and the overall oxidation kinetics progressive accelerates. One aim of the

present study is to bring insights into the underlying metallurgical evolutions responsible for the complex oxidation kinetics of Cr-coated zirconium-based alloys oxidized in steam at temperatures up to 1500°C. For that purpose, detailed post-oxidation microstructural examinations have been carried out in order to explain the three main oxidation steps defined in Figure 1. Special attention is paid to oxygen diffusion into the zirconium metallic substrate, because it is well known that this is one first order parameter influencing the post-HT oxidation and quenching mechanical properties of zirconium-based claddings.

2. MATERIALS AND EXPERIMENTAL PROCEDURES

2.1 Materials

As a first step, the Cr-coatings have been deposited by PVD on 1.2mm-thick low-tin Zircaloy-4 sheet samples. The typical Cr-coating thicknesses range between 5 and 10µm. In the following, these early Cr-coated produced materials are defined as the first generation Cr-coated Zr. Typical grain morphologies and associated crystallographic textures of the first generation Cr-coating are illustrated in Figure 2. More recently, 10 to 20µm-thick coatings were deposited onto the outer surface of $M5_{Framatome}$ cladding tubes, with typical outer diameter and thickness of 9.5 and 0.57 mm, respectively.

At that point, it must be mentioned that, in the following, the experimental results shown correspond to different types of Cr-coated samples, from the first generation Cr-coated Zircaloy-4 sheets to the last generation $M5_{Framatome}$ tubular cladding geometry, with different coating thicknesses and as-received microstructures. On the one hand, as discussed further hereinafter, the HT oxidation kinetics process may depend on the as-received Cr-coating grain size. On the other hand, the effect of the initial Cr-coating crystallographic texture is more difficult to establish because the texture changes continuously upon incursion at HT due to Cr grain recrystallization.

However, more details on the as-received Cr-coated materials microstructures and properties are given in [7] and [12]. Additional insights into the structure of the Cr-coating / Zr substrate interface, down to the atomic scale, can be found in [51]. For this last case, it has been shown that, for the PVD coatings developed here, the Cr-Zr interface appears to be defects-free with crystallinity continuity between the two polycrystalline materials, thus insuring a very good Cr-Zr bounding.

2.2 High temperature steam oxidation

One-sided (for tubular geometry) and two-sided (for sheet geometry) isothermal oxidation tests were performed in flowing steam at atmospheric pressure, at various temperatures between 800 and 1500°C. Three different oxidation and quenching facilities have been used:

- the CEA's DEZIROX 1 facility, on which more than two thousand tests have been conducted so far [33]-[36];
- the HT oxidation test facility recently developed at Framatome-Paimboeuf, with technical characteristics close to those of DEZIROX1 [37];
- the new CEA's HT steam oxidation facility called I2TOx, able to perform HT tests under inert or controlled steam environment at temperatures up to 1600°C. In this new experimental device, complex thermal cycling can be applied with continuous control of sample temperature, gas flow and humidity, and with fully automatized final water quenching. For the present study, a heating rate of 1°C/s has been applied. Heating began under flowing helium (neutral environment) and steam was introduced at 600°C or at 1300°C until the end of the tests (final water quenching).

For the three HT oxidation devices used, the steam flux was high enough to avoid steam starvation or significant temperature overshoot due to the exothermic HT oxidation of the tested materials.

2.3 Post-HT oxidation/quenching examinations

Post-HT oxidation hydrogen content measurements (three measurements per sample) were carried out using a HORIBA EMGA-821 analyser.

Electron Probe Micro-Analysis (EPMA, CAMECA SX100 electron microprobe) was carried out after oxidation and quenching to get additional insights into the potential oxygen (and other chemical species such as chromium) diffusion into the Zr-based substrate. Indeed, it is well known that the Post-Quenching (PQ) mechanical properties of the cladding and thus its potential embrittlement rely on the thickness and the oxygen content of the residual prior-β_{Zr} layer [35] [38]-[40].

Detailed microstructural PQ examinations were carried out from the microscale, using Scanning Electron Microscopy (SEM) coupled with Electron Back Scattered Diffraction (EBSD) analysis, down to the nanoscale, using High Resolution Transmission Electron Microscopy (HRTEM). For this last case, TEM specimens were prepared using Gallium Focused Ion Beam (FIB) after platinum metallization and platinum deposition with ion beam. 30µm-long and 20µm-deep sections of the samples were extracted, glued on copper grids, and then thinned with FIB at decreasing voltages and currents. Prior to TEM observation, lamellas were previously cleaned at low voltage and low current with Gallium FIB.

3. RESULTS AND DISCUSSION FOR OXIDATION AT TEMPERATURES UP TO 1300°C

3.1 Beginning of oxidation (protective coating)

As already mentioned in [7], the Cr-coatings studied here are fully protective at the beginning of oxidation. Thus, for typical DBA and slightly beyond LOCA conditions, growth of the outer chromia scale under isothermal conditions should be described using a parabolic law (Equation 1):

$$X_{Cr2O3} = (K_p.t)^{1/2} \quad \text{- Equation 1}$$

where X_{Cr2O3} is the thickness of the outer chromia scale, t is the oxidation time and K_p is the parabolic rate constant.

The values of K_p (in $cm^2.s^{-1}$) obtained for oxidation temperatures ranging from 800 up to 1300°C are shown in Figure 3, where they are compared to values reported in the literature for HT oxidation of pure (bulk) chromium in oxygen or air environments [41]-[49]. One can observe that the K_p values reported in the literature for pure chromium are distributed over several orders of magnitude. It has been shown that under atmospheres containing O_2, chromia grows by diffusion of species across the oxide scale. Short-circuit diffusion paths such as grain boundaries in oxide scales may have a major effect on the oxidation kinetics [49], which could contribute to the large scatter of the data. Nevertheless, the K_p values obtained in the present study for Cr-coatings tested upon steam at HT and for short oxidation times are consistent with the quite recent experimental values from Taneichi *et al.* [48] and with the ones calculated by Atkinson [47] using the diffusion coefficient of polycrystalline chromia reported by Hagel and Seybolt [43].

At this point, it must be mentioned that part of the metallic chromium reacting with oxygen at HT may volatilize (*i.e.*, by formation of CrO_3 and/or of volatile gaseous species such as $CrO_2(OH)_2$ and CrO_2OH), which would induce a weight loss. For example, such a phenomenon has been proposed recently by Yeom *et al.* [76] to explain the observed sub-parabolic (*i.e.*, quartic) oxidation kinetics of cold spray Cr coatings at 1230°C and above. However, a weight loss of approximately 0.04 mg/cm²/h due to chromium volatilization has been measured for pure chromium upon oxidation at 1300°C at atmospheric pressure, for long oxidation [50]. This value is at least two orders of magnitude lower than the weight gain values measured on Cr-coatings in the present study at short oxidation times, associated with the growth of an outer chromia scale. Nevertheless, to assess the assumption of negligible contribution of the HT volatilization of the Cr oxide for the HT oxidation conditions experienced here, an experimental

equivalent post-oxidation chromium metallic thickness has been calculated by adding the thicknesses of:

(i) the residual chromium metallic layer measured after oxidation,
(ii) the chromia scale measured after oxidation divided by the Pilling-Bedworth coefficient for Cr-Cr_2O_3 (approximately 2 for dense chromia),
(iii) Cr obtained by integrating the overall quantity of prior-metallic-chromium that has diffused into the β_{Zr} substrate measured by EPMA or calculated as reported in [7].

As illustrated in Figure 4, it was observed that the recalculated equivalent post-oxidation metallic chromium thicknesses are equal or slightly larger than the measured initial (as-received) thicknesses. Thus, for the HT oxidation conditions tested here, it is assumed that the contribution of chromium volatilization can be neglected.

Typical microstructures obtained for the first generation of 5-10µm-thick Cr-coated Zircaloy-4 sheet samples after steam oxidation for 300s at 1200°C and water quenching are shown in Figure 5. Three outer layers are highlighted:

(1) An outer chromia scale with submicronic grains. This oxide scale displays a typical Cr_2O_3 rhombohedral crystallographic structure with a particular crystallographic texture, the (001) crystallographic planes being mainly perpendicular to the coating surface. TEM micrographs in Figure 6 show that the bulk outer chromia scale is dense, without apparent defects or cracks, while numerous cavities are observed at the chromium oxide/metal interface. One may assume that those cavities have been produced by a Kirkendall-type mechanism due to the outward cationic diffusion of Cr from the sub-oxide Cr metallic layer, inducing back diffusion of vacancies at the Cr_2O_3/Cr interface. Additionally, as it will be shown further, oxygen inward diffusion throughout the remaining sub-oxide metallic chromium layer should also contribute to the production of vacancies at the oxide (chromia)-metallic (chromium) interface, and thus to the nucleation and growth of Kirkendall cavities at this interface. However, as discussed below, in this case, oxygen diffusion occurs at the boundaries of the prior-chromium grains. Consequently, one could assume that this heterogeneous (intergranular) oxygen diffusion mechanism is less susceptible to induce a high density of Kirkendall cavities at the chromia-metallic chromium interface, because grain boundaries are known to be efficient recombining/annihilation sites for vacancies. Then, even if it cannot be ignored, the inward intergranular oxygen diffusion mechanism in prior-chromium appears to be less efficient than the outward cationic volume diffusion mechanism in chromium for formation of back-vacancies and thus Kirkendall cavities at the chromia/chromium interface. Moreover, HRTEM micrographs in Figure 6-(c) reveal a certain crystallographic coherency between the neighboring chromia grains. This confirms the high density and the defect-free structure of the formed outer chromia scale. This explains the efficient protective properties of the coating observed at the beginning of oxidation for a fully dense coating.
(2) A sub-oxide residual metallic chromium layer with micrometer-sized grains showing a fiber-type crystallographic texture with the (100) direction of the body centered cubic (bcc) structure perpendicular to the coating surface. It is likely that this particular texture has been inherited from the as-received crystallographic texture induced by the PVD deposition process.
(3) A continuous chromium-zirconium micrometer-thick layer at the Cr/prior-β_{Zr} interface. This layer is due to the inter-diffusion between the Zr substrate and the Cr coating occurring upon the incursion at HT. Consistently with the Zr-Cr phase diagram, it was observed that this thin layer is constituted mainly of an intermetallic $Zr(Cr,Fe)_2$ C15 (face centered cubic, fcc) Laves phase. As already observed and discussed in [51] and [52], a slight enrichment in Fe of this Zr-Cr interface intermetallic layer is sometimes observed. This could explain why, for slightly longer oxidation times (next section of this paper), the C14 (hexagonal close packed, hcp) intermetallic is observed by TEM (Figure 7-(b)-right). This can be related to the high thermodynamic affinity of the C14 Laves phase with Fe and to the quite fast diffusion of Fe from the substrate, after full

dissolution of the intermetallic secondary phases precipitates of the Zircaloy-4 matrix at such HT. From EBSD analysis, the intermetallic grains display no significant overall crystallographic texture (*i.e.*, nearly isotropic distribution). Moreover, one can observe on EBSD orientation maps (Figure 5-(b)) the typical twinned intermetallic Laves phase substructure. Furthermore, cavities are observed at the intermetallic/zirconium interface. Again, one can assume that these cavities have been produced by a Kirkendall effect but here, at the Cr-Zr metallic interface: at 1200°C, the solubility and diffusivity of chromium in β_{Zr} are expected to be much higher than the ones of zirconium in chromium. This induces an inward diffusion of metallic Cr atoms within the β_{Zr} substrate significantly larger than the potential outward diffusion of zirconium atoms within the Cr layer. Then, the dissymmetric atomic diffusion at both sides of the Zr/Cr interface induces a back diffusion flux of vacancies from the β_{Zr} substrate. Finally, clustering and coalescence of Kirkendall vacancies promote nucleation and growth of the observed interfacial cavities (a few tenths of nanometers in diameter).

3.2 Transition between protective and non-protective coating

This transition is characterized by a progressive and smooth acceleration of the weight gain evolution, the growth rate of the outer chromia drastically decreasing. As already discussed, this phenomenon is unlikely to be related to chromium volatilization. This means that, at this oxidation stage, a significant fraction of the oxygen reacting with the Cr-coated material (which contributes to the positive weight gain evolution measured) diffuses deeper into the sub-chromium oxide substrate. Indeed, as illustrated in Figure 7, post-oxidation EBSD and TEM examinations showed that a new oxygen transport mechanism is activated beneath the chromium oxide layer:

- Inward oxygen diffusion together with outward zirconium intergranular diffusion occur within the residual metallic chromium layer.
- Then, zirconia stringers nucleate and grow at the chromium grain boundaries, likely due to the higher thermodynamic stability of zirconia compared to chromia.
- Thus, it can be assumed that this more or less continuous network of zirconia at chromium grain boundaries promotes (inward) diffusion of oxygen anions.

This proposition of mechanism is supported by the EBSD map in Figure 7 which clearly shows that, when the oxygen atoms diffusing inward along grain boundaries reach the Zr/Cr interface, oxygen-stabilized $\alpha_{Zr}(O)$ incursions form within the β_{Zr} substrate. Moreover, it is worth noticing that $\alpha_{Zr}(O)$ nucleates and grows in the extent of the adjacent chromium grain boundaries (decorated by zirconia stringers). This supports again the oxygen transport mechanism proposed above.

Finally, it can be observed in Figure 7 that, at this oxidation stage, the interfacial intermetallic $Zr(Cr,Fe)_2$ layer is still present and has grown significantly. The typical thickness of this layer (*i.e.*, ~1.5-2µm) is consistent with the kinetics data reported for such diffusion couple systems when extrapolated at 1200°C [53][54].

3.3 Longer oxidation times (no longer protective coating)

Figure 8 shows the typical PQ microstructure of a ~5µm-thick Cr-coated Zircaloy-4 sample heavily oxidized. At this stage and due to its limited initial thickness, the residual Cr-coating is no longer protective so that a thick zirconia layer grows beneath the heavily oxidized residual Cr-coating. This is associated with a significant acceleration of the overall oxidation kinetics (non-protective Zr substrate oxidation). The different layers observed on the EBSD maps shown in Figure 8 are the following:

- An outer heavily damaged residual chromia scale. The numerous cracks and potential local delamination of the residual outer Cr oxide scale show that the scale is definitely no more protective at this stage.
- An underlying residual metallic (not oxidized) chromium layer, showing a quasi-continuous intergranular zirconia network. As discussed previously, it is likely that this zirconia network is a preferential path for an accelerated access of oxygen to the zirconium substrate.

- Probably because of the high inward diffusion flux of oxygen at the Zr/Cr interface when the coating is no more protective, it can be observed that the (prior-)$Zr(Cr,Fe)_2$ layer has disappeared and transformed back into metallic chromium grains together with zirconia grains, according to the assumed chemical reaction described below (Equation 2, *the slight contribution of Fe is neglected*):

$$Zr(Cr)_2 + 2O \Rightarrow ZrO_2 + 2Cr \quad \text{- Equation 2}$$

  This last observation is consistent with the recent findings from Han *et al.* [71]. However, even if there are some analogies, their findings do not exactly apply here because, in the present study, there is still an outer metallic (un-oxidized) chromia scale that remains while a thick sub-coating zirconia layer has already grown (Figure 8). One may assume that for the longest oxidation times experienced here, all oxygen atoms reacting with the clad surface diffuse preferentially by the zirconia short-path network (formed into the remaining chromium sub-chromia layer) into the zirconium substrate, inducing growth of a thick zirconia scale and thus keeping the neighboring metallic chromium un-oxidized.
- Finally, a thick zirconia layer is observed beneath the residual chromium-rich outer layers. Figure 8 shows the typical PQ morphological and crystallographic textures of zirconium oxide. One can assume that this particular oxide microstructure is due to:
  (1) formation during oxidation at 1200°C of coarse columnar tetragonal zirconia grains (*at 1200°C, zirconia is expected to be fully tetragonal [75]*);
  (2) transformation of tetragonal zirconia into (sub-grains) monoclinic crystallographic variants upon the final quenching down to room temperature. The particular “periodic oriented bands” morphology of zirconia sub-grains should rely on the orientation relationships between the former tetragonal phase and the resultant monoclinic phase [55]. Indeed, the associated pole figure (Figure 8-B-right) highlights a specific crystallographic texture for PQ zirconia, likely inherited from the crystallographic texture of the former tetragonal grains formed at HT. However, a deeper analysis and discussion of the crystallographic and morphological textures of the zirconia scale formed at HT is out of the scope of the present paper.

3.4 Effect of chromium grain size and morphology

To get more insights and to assess the phenomenological oxidation mechanism proposed herein, pre-annealing thermal treatments under neutral environment (secondary vacuum) have been carried out on 6-8µm-thick Cr-coated Zr1Nb(O) (sheets materials) for 2 hours at both 700 and 800°C. As shown in Figure 9, the idea here was to increase the initial chromium grain size and thus to decrease the density of grain boundaries. Indeed, as observed above, grain boundaries may constitute preferential paths for oxygen diffusion for intermediate and long HT oxidation times.

Subsequently, the as-received and annealed coated samples were subjected to steam oxidation for 1500s at 1200°C and then water quenched down to RT. This particular oxidation time at 1200°C has been chosen because, for 6-8µm-thick Cr coatings, it corresponds more or less to the beginning of the non longer protective HT oxidation process (*i.e.*, formation of fresh zirconia layer beneath the residual coating).

Figure 10 and Figure 11 confirm that pre-annealing (chromium recrystallization) has a delaying effect on oxidation at HT. Indeed, it is observed that as the annealing temperature and thus the chromium grain size increase, the subsequent oxidation and the associated oxygen ingress into the Zr substrate are significantly reduced when compared to the behavior of the as-deposited material. These results seem to confirm the significant contribution of the grain boundaries of the (metallic) chromium to the oxygen diffusion/transport into the zirconium substrate for longer oxidation times.

This higher chromium grain size (and morphology) effect may have positive consequences during hypothetical accidental transients during which the nuclear fuel clad may stay a certain time at

intermediate temperatures (~600-1000°C) before reaching the higher PCT. Indeed, the resistance of the Cr coating to HT oxidation when reaching PCT may be increased due to the decrease of the density of chromium grain boundaries during prior holding at intermediate temperatures, limiting short-circuit paths for diffusion of oxygen through the residual (un-oxidized) chromium metallic layer. It is also possible that the chromium coating recrystallization that occurs upon annealing modifies the Cr grain boundary atomic arrangement / energy and its intrinsic atomic transport properties, thus decreasing the overall grain boundary diffusion coefficients of chemical species (zirconium and/or oxygen) and/or increasing the energy barrier for intergranular nucleation of zirconia.

3.5 Hydrogen uptake

Upon steam oxidation at 1200°C under atmospheric pressure and as far as the steam flux is high enough to prevent from steam starvation, no significant hydrogen uptake is usually observed for modern uncoated nuclear zirconium-based fuel claddings [56]. In other words, the outer (tetragonal) zirconium oxide scale formed in these conditions is dense and constitutes an efficient hydrogen permeation barrier.

Systematic PQ hydrogen analysis have been performed on ~15µm-thick Cr-coated zirconium alloys after steam oxidation up to a few hours, at both 1200°C and 1300°C. To be able to rationalize and to compare the results obtained at these two different oxidation temperatures, one can use the Equivalent Cladding Reacted (ECR) parameter instead of the oxidation time. The zirconium-based alloy ECR parameter is defined as the fraction of zirconium consumed (in relation to the initial thickness of the metallic clad) if all the oxygen having reacted with the cladding during oxidation and having diffused through the material had led to the formation of stoichiometric ZrO_2. The historical background of the ECR-related regulatory LOCA criteria and a discussion about these criteria can be found in refs. [57]-[59]. An ECR limit of 17% preventing uncoated Zr-based claddings from detrimental embrittlement, associated with the Baker-Just (BJ) correlation describing the oxidation kinetics of uncoated Zircaloy-4 under steam at HT [60], was derived from the early work performed in the 1960s and the early 1970s [61]-[63].

The PQ hydrogen contents (in weight-ppm, wt.ppm) and the sub-coating zirconia thicknesses measured for 12-15µm-thick Cr-coated Zr-based materials after one-sided steam oxidation at 1200 and 1300°C are given in Table **1** for the different oxidation times tested. The corresponding calculated ECR-BJ values (related to uncoated Zircaloy-4) are also mentioned. The evolution of the PQ hydrogen content and of the (under-residual-coating) zirconia layer thickness measured on Cr-coated materials are plotted in Figure 12 as a function of the calculated ECR-BJ for steam oxidation at both 1200°C and 1300°C. A transient hydrogen uptake corresponding to a quite short period is observed when the coating becomes fully non-protective. It can be assumed that there is a short time-period during which steam has a direct access to the metallic zirconium-based substrate, when the Cr-coating loses definitely its protective properties, which may coincide with the early formation of thin and discontinuous zirconia spots beneath the residual Cr-coating. Nevertheless, this phenomenon occurs at high ECR values (*i.e.* between approximately 50 and 60%, for the uncoated material) and appears to be limited to a hydrogen uptake of a few hundreds of wt.ppm. The hydrogen content saturates after this short transient period.

Indeed, when the chromium coating loses its protective properties after a long oxidation period and despite a short transient and limited hydrogen uptake, the continuous zirconia layer formed at HT beneath the residual Cr-coating appears to be dense and protective against further hydrogen uptake.

3.6 Summary

Before describing the HT oxidation mechanism of Cr-coated zirconium alloys, it is useful to recall the fundamental characteristics of oxygen diffusion in the uncoated reference materials upon HT oxidation. Figure 13 depicts the different layers formed upon HT oxidation on uncoated reference zirconium-based alloys and the associated oxygen diffusion profile (schematic plot derived from [64]). One-dimension oxygen diffusion modelling has been developed, based on both analytical and numerical approaches [65]-[69]. For short oxidation times (isothermal conditions) and except for post-breakaway oxidation or steam starvation situations, the growth kinetics of the outer zirconia scale and the intermediate $\alpha_{Zr}(O)$ layer are nearly parabolic.

Figure 14 is a schematic overview of the different stages of the HT steam oxidation process of Cr-coated zirconium-based alloys (the additional transient hydrogen diffusion/uptake is not considered here for sake of simplicity).

Finally, it must be mentioned that specific HT oxidation mechanisms have been reported for titanium-based substrate [70] and, more recently, and as already mentioned, for Cr-coated zirconium-based substrate [71]. However, to our knowledge, the oxidation mechanism that has been observed here, involving outward intergranular diffusion of zirconium through the residual metallic (un-oxidized) chromium layer with subsequent formation of a zirconia intergranular network and transient hydrogen uptake, had never been reported before. Further experimental study and modelling efforts are planned to get a deeper understanding of the present underlying diffusion mechanism.

4. RESULTS FOR OXIDATION AT TEMPERATURES HIGHER THAN 1300°C

For oxidation temperatures higher than 1300°C, a eutectic reaction may occur between pure zirconium and chromium with a theoretical eutectic temperature close to 1332°C, according to the binary Zr-Cr phase diagram. In case of formation of a eutectic liquid outer layer, the HT steam oxidation behavior of Cr-coated zirconium alloys is questionable. To investigate the effect of a eutectic liquid outer layer on the actual HT steam oxidation behavior of Cr-coated zirconium alloys, preliminary studies have been recently carried out [17][72]. The main findings from [17] are summarized hereinafter. Then the mechanisms of HT steam oxidation of Cr-coated Zr alloys are described when a Zr-Cr eutectic reaction has occurred.

Before carrying out steam oxidation tests at very HT (≥1300°C), calorimetric measurements have been performed under (inert) helium gas on Cr-coated $M5_{Framatome}$ to determine the temperatures at which the eutectic Zr-Cr reaction occurs. Heating and cooling rates of 10°C/min have been applied, corresponding to near equilibrium conditions. A part of the thermogram obtained is shown in Figure 15-(b). The Zr-Cr eutectic reaction is clearly highlighted by an endothermic peak between ~1305°C and ~1325°C. It has been checked that the associated measured enthalpy is consistent with the melting enthalpy of pure zirconium. Additionally, Figure 15-(c) and Figure 15-(d) illustrate the typical post-test eutectic microstructure and micro-chemical profiles obtained by EPMA. As anticipated from the equilibrium phase diagram (Figure 15-(a)), the eutectic liquid phase has decomposed during the slow cooling into prior-β_{Zr} (enriched in oxygen) and $ZrCr_2$ intermetallic phases.

Then, steam oxidation tests have been conducted up to 1500°C for short exposure times on coated and uncoated $M5_{Framatome}$ industrial clad segments, followed by direct water quenching. For the conditions tested and as described in more details in [17], Cr-coated clad segments did not fail upon the final water quenching while some uncoated reference segments did. To get more insights into the microstructural and micro-chemical evolution of the tested Cr-coated $M5_{Framatome}$ clad segments, detailed PQ metallurgical examinations were carried out.

Figure 16 shows the typical PQ aspect of the coated samples after one-sided HT steam oxidation at temperatures above the temperatures at which the Zr-Cr eutectic reaction occurs (~1305-1325°C according to differential scanning calorimetry measurements performed under neutral environment

(pure flowing argon [17]). For such very HT oxidation conditions, the PQ Cr-coated clad surface shows a “crocodile skin” morphology with some continuous blisters forming an external protruding pattern. This “crocodile skin” aspect should be due to small displacement of the Zr-Cr eutectic film at the outer clad surface, induced by potential liquid “capillary” effects and local swelling associated with the solid-to-liquid volume change.

Figure 17 shows an example of EPMA results at the location of one protruding blister. From the mapping of oxygen and chromium, one can observe that the protruding blister corresponds to the formation at HT of a prior-liquid “pocket” with a typical dendritic substructure generated upon the final solidification/quenching. This zone consists of both chromium-depleted prior-β_{Zr} dendrites and chromium-enriched inter-dendritic zones, containing around 30at.% of chromium. Such microstructure can be understood by considering the pseudo-binary $M5_{Framatome}$-Cr phase diagram shown in Figure 18. This phase diagram has been calculated using the Thermocalc® software and the CEA’s Zircobase thermodynamic database for zirconium alloys [73][74]. The various metallurgical evolutions upon heating beyond 1300°C, annealing for 100s at ~1400-1450°C and final water quenching down to room temperature, can be summarized as follows:

(a) upon heating beyond 1300°C, fast inter-diffusion between Zr and Cr occurs, then the intermediate metallic $ZrCr_2$ layer reacts with the β_{Zr} substrate to form the eutectic liquid phase;

(b) upon annealing for 100s at 1400-1450°C, the liquid (eutectic) phase is progressively enriched in zirconium coming from the Zr-substrate (considering that no more Cr is available due to its early consumption to form a eutectic liquid phase upon heating in the 1305-1325°C temperature range);

(c) upon quenching from 1400-1450°C, β_{Zr} dendrites precipitate in association with enrichment in Cr of the inter-dendritic residual Zr-Cr liquid phase as the temperature decreases; then, the residual Zr-Cr liquid phase solidifies when the temperature decreases below the eutectic point of the phase diagram, which corresponds to approximately 30%at. of chromium, consistently with EPMA measurements.

Additionally, EPMA oxygen mapping shows that continuous outer scales of ZrO_2 and $\alpha_{Zr}(O)$ have grown during the HT oxidation process. The homogeneity and uniformity of these outer scales are remarkable. The local oxidation kinetics are outstandingly the same at the liquid eutectic and the Cr-depleted locations. This indicates that the formation of a liquid Zr-Cr phase at the outer surface of the Cr-coated clad at temperatures higher than 1300°C may not drastically modify the HT oxidation mechanisms and kinetics of the zirconium-based material, at least for the quite short oxidation times experienced here.

5. CONCLUSIONS

Chromium-coated zirconium-based claddings are studied as potential near-term EATF for LWRs. Previous studies have shown that, as far as appropriate deposition process/parameters and coating thicknesses are used, the Cr-coating is able to induce significant additional “grace period” before oxidation becomes too severe in LOCA conditions up to at least 1300°C.

Zircaloy-4 sheet samples with 5-10µm-thick Cr-coatings and $M5_{Framatome}$ cladding samples with 10-20µm-thick outer Cr-coatings deposited using a special PVD process were oxidized in flowing steam (atmospheric pressure) at various temperatures between 800 and 1500°C. The samples were then examined in depth after oxidation and quenching. For oxidation temperature up to 1300°C, it is shown that the overall oxidation kinetics can be divided into three main successive stages, corresponding to different underlying oxidation/diffusion mechanisms:

Protective coating oxidation: This early stage corresponds to a nearly parabolic oxidation kinetics with growth of an outer protective chromia scale. Parabolic rate constants for Cr_2O_3 have been determined within the 800-1300°C steam oxidation temperature range. The obtained values are consistent with data previously published obtained on bulk chromium upon HT oxidation in oxygen or air. After HT oxidation

and quenching, EBSD and HR TEM examinations were carried out. Chromia appears to be dense (with a specific crystallographic texture), in accordance to its protectiveness nature. At the Zr/Cr interface and due to thermally-accelerated Zr-Cr inter-diffusion, thickening of a $Zr(Cr,Fe)_2$ inter-layer is also observed and, as already reported and discussed in [7], inward volume diffusion of Cr occurs within the prior-β_{Zr} substrate, thus contributing to the overall thinning of the Cr-coating.

Transition: This oxidation transition time-period is characterized by a smooth acceleration of the weight gain evolution. Additionally, the outer chromia thickening rate drastically decreases. As discussed and evidenced in the paper, it is unlikely that this phenomenon is related to chromium volatilization. In-depth post-oxidation examinations showed that, during this transition time-period, a fraction of the oxygen reacting with the Cr-coated material diffuses deeper into the sub-chromia substrate throughout the residual metallic (un-oxidized) chromium thickness. It is shown that this progressive oxygen ingress into the zirconium substrate is due to an outward diffusion of Zr along chromium grain boundaries. This induces formation of zirconia layers at chromium grain boundaries, promoting further inward oxygen diffusion.

Non-protective coating oxidation: When the protectiveness of the Cr-coating is lost, a significant acceleration of the overall oxidation kinetics is observed, associated with a transient hydrogen uptake. At this stage, since the residual Cr-coating is no longer protective, a thick zirconia layer grows beneath the heavily oxidized residual Cr-coating. EBSD examinations showed that the zirconia layer with *a priori* a tetragonal structure at HT (with a columnar morphology) displays characteristic sub-grains corresponding to monoclinic crystallographic variants after cooling. Additionally, probably because of the high inward diffusion flux of oxygen at the Zr/Cr interface, the prior-$Zr(Cr,Fe)_2$ inter-layer disappears and transforms back into metallic chromium grains together with zirconia grains, according to the assumed chemical reaction: $Zr(Cr)_2 + 2O \Rightarrow ZrO_2 + 2Cr$.

To get more insights into the mechanisms involved, Cr-coated Zr-based samples were pre-annealed under neutral environment at 700-800°C to increase the initial chromium grain size and thus to decrease the initial density of grain boundaries of the chromium coating. It is observed that, as the pre-annealing temperature and thus the chromium grain size increase, HT oxidation and associated oxygen ingress into the Zr substrate are significantly reduced. This suggests that the (metallic) chromium grain boundaries significantly contribute to the oxygen diffusion/transport throughout the thickness of the residual (un-oxidized) metallic chromium layer towards the zirconium substrate.

HT steam oxidation experiments carried out at temperatures above 1300°C show that the formation of a liquid Zr-Cr (eutectic) phase at the outer surface of the Cr-coated clad may not drastically modify the HT oxidation mechanisms and kinetics of the zirconium-based material, at least for the quite short oxidation times experienced here.

ACKNOWLEDGEMENTS:

Numerous people took part to this study at CEA and the authors want to thank them all.

Special thanks to:

- M. Le Flem and I. Idarraga (*now at EDF-DT*) from CEA for their initial input on R&D on coated Zr-based alloys;
- D. Hamon from CEA, for EPMA measurements;
- F. Lomello, A. Michau and F. Schuster from CEA, G. Velisa and A. Billard from UTBM (Montbéliard, France) and E. Monsifrot and J. Runser from the DEPHIS society (Etupes, France), for PVD Cr-coated materials fabrication;
- T. Forgeron, P. Bossis, J. Henry, L. Vincent, L. Portier and A. Soniak from CEA, for their advising and organizing support.

This study has been partially conducted under the french three-parties nuclear institute between CEA, Framatome and EDF. Specific thanks to C. Delafoy from Framatome and N. Waeckel from EDF.

DATA AVAILABILITY:

The raw/processed data required to reproduce these findings cannot be shared at this time due to technical or time limitations.

REFERENCES

[1] S.J. Zinkle, K.A. Terrani, J.C. Gehin, L.J. Ott, L.L. Snead, “Accident tolerant fuels for LWRs: A perspective”, Journal of Nuclear Materials 448 (2014), 374–379

[2] Y.-H. Koo, J.-H. Yang, J.-Y. Park, K.-S. Kim, H.-G. Kim, D.-J. Kim, et al., “KAERI’s development of LWR accident tolerant fuel”, Nucl. Technol. 186 (2014) 295–30

[3] M. Kurata, “Research and development methodology for practical use of accident tolerant fuel in light water reactors”, Nucl. Eng. Technol. 48, (2016), 26–32

[4] Z. Duan, H. Yang, Y. Satoh, K. Murakami, S. Kano, Z. Zhao, J. Shen, H. Abe, “Current status of materials development of nuclear fuel cladding tubes, for light water reactors”, Nuclear Engineering and Design 316 (2017) 131–150

[5] K. A. Terrani, “Accident tolerant fuel cladding development: Promise, status, and challenges”, Journal of Nuclear Materials 501 (2018) 13–30

[6] State-of-the-art Report on Light Water Reactor Accident Tolerant Fuel: Cladding, Core Materials and Advanced Fuel Designs, OECD, NEA Report n°7317 (2018)

[7] J.C. Brachet, I. Idarraga-Trujillo, M. Le Flem, M. Le Saux, V. Vandenberghe, S. Urvoy, E. Rouesne, T. Guilbert, C. Toffolon-Masclet, M. Tupin, C. Phalippou, F. Lomello, F. Schuster, A. Billard, G. Velisa, C. Ducros, F. Sanchette, “Early studies on Cr-Coated Zircaloy-4 as Enhanced Accident Tolerant Nuclear Fuel Claddings for Light Water Reactors”, Journal of Nuclear Materials 517 (2019) 268–285

[8] I. Idarraga-trujillo, M. Le Flem, J-C Brachet, M. Le Saux, D. Hamon, S. Muller, V. Vandenberghe, M. Tupin, E. Papin, A. Billard, E. Monsifrot, F. Schuster, “Assessment at CEA of Coated Nuclear Fuel Cladding for LWRs with Increased Margins in LOCA and beyond LOCA Conditions”, Proceedings of 2013 LWR Fuel Performance Meeting/TopFuel, Charlotte, NC, USA, Sept. 15-19, (2013)

[9] J. Bischoff, K. McCoy, J. Strumpell, J-C. Brachet, C. Lorrette, "Development of Fuels with Enhanced Accident Tolerance", Proceedings of TopFuel Conference 2015, Zurich, Switzerland, (Sept. 2015)

[10] J.C. Brachet, M. Le Saux, M. Le Flem, S. Urvoy, E. Rouesne, T.Guilbert, C. Cobac, F. Lahogue, J. Rousselot, M. Tupin, P. Billaud, C. Hossepied, F. Schuster, F. Lomello, A. Billard, G. Velisa, E. Monsifrot, J. Bischoff, A. Ambard, "On-going Studies at CEA on Chromium Coated Zirconium-based Nuclear Fuel Claddings for Enhanced Accident Tolerant LWR Fuel", Proceedings of TopFuel Conference 2015, Zurich, Switzerland, (September 2015)

[11] J. Bischoff, C. Delafoy, P. Barberis, D. Perche, B. Buerin, J-C Brachet, "Development of Cr-coated Zirconium Cladding for Enhanced Accident Tolerance", Proceedings of TopFuel Conference 2016, Boise, ID, USA, (September 2016)

[12] J. Bischoff, C. Delafoy, C. Vauglin, P. Barberis, C. Roubeyrie, D. Perche, D. Duthoo, F. Schuster, J-C. Brachet, E.W. Schweitzer, K. Nimishakavi, "AREVA NP's Enhanced Accident Tolerant Fuel Developments: Focus on Cr-coated M5 Cladding", Nuclear Engineering and Technology 50 (2018) 223-228

[13] J. Bischoff, C. Delafoy, N. Chaari, C. Vauglin, K. Buchanan, P. Barberis, F. Schuster, J-C Brachet, K. Nimishakavi, “Cr-coated cladding development at Framatome”, Proceedings of WRFPM/TOPFUEL 2018, Prague, Czech Republic, (30 Sept. – 04 Oct. 2018)

[14] J.C. Brachet, M. Le Saux, V. Lezaud-Chaillioux, M. Dumerval, Q. Houmaire, F. Lomello, F. Schuster, E. Monsifrot, J. Bischoff, E. Pouillier, "Behavior under LOCA Conditions of Enhanced Accident Tolerant Chromium Coated Zircaloy-4 Claddings", Proceedings of TopFuel 2016 Conference, Boise, ID, USA, (September 2016)

[15] J.C. Brachet, M. Dumerval, V. Lezaud-Chaillioux, M. Le Saux, E. Rouesne, D. Hamon, S. Urvoy, T. Guilbert, Q. Houmaire, C. Cobac, G. Nony, J. Rousselot, F. Lomello, F. Schuster, H. Palancher, J. Bischoff, E. Pouillier, "Behavior of Chromium Coated M5 Claddings under LOCA Conditions" Proceedings of WRFPM Conference, Jeju, Republic of South Korea, (September 2017)

[16] C. Delafoy, J. Bischoff, J. Larocque, P. Attal, L. Gerken, K. Nimishakavi, “Benefits of Framatome’s EATF evolutionary solution: Cr-coated cladding with Cr2O3-doped UO2 fuel”, Proceedings of TopFuel 2018, Prague, Czech Republic, September 2018

[17] J.C. Brachet, T. Guilbert, M. Le Saux, J. Rousselot, G. Nony, C. Toffolon-Masclet, A. Michau, F. Schuster, H. Palancher, J. Bischoff, J. Augereau, E. Pouillier, “Behavior of Cr-coated M5 claddings during and after high temperature steam oxidation from 800°C up to 1500°C (LOss-of-Coolant Accident & Design Extension Conditions)”, Proceedings of WRFPM/TOPFUEL 2018, (30 Sept. – 04 Oct. 2018), Prague, Czech Republic

[18] J.C. Brachet, T. Guilbert, S. Urvoy, M. Le Saux, G. Nony, T. Vandenberghe, A. Lequien, C. Miton, J. Bischoff, E. Pouillier, “Relationship between Equivalent Cladding Reacted parameters, and post-quenching ductility of Cr-coated M5 fuel claddings steam oxidized at 1200 and 1300°C”, submitted to Journal of Nuclear Materials (2019)

[19] C. Tang, M. Stueber, H.J. Seifert, M. Steinbrueck, “Protective coatings on zirconium-based alloys as accident tolerant fuel (ATF) claddings”, Corros. Rev. 35 (2017) 141–165

[20] H.-G. Kim, I.-H. Kim, Y.-I. Jung, D.-J. Park, J.-Y. Park, Y.-H. Koo, “Adhesion property and high-temperature oxidation behavior of Cr-coated Zircaloy-4 cladding tube prepared by 3D laser coating”, J. Nucl. Mater. 465 (2015) 531–539

[21] A.S. Kuprin, V.A. Belous, V.N. Voyevodin, V.V. Bryk, R.L. Vasilenko, V.D. Ovcharenko, et al., “Vacuum-arc chromium-based coatings for protection of zirconium alloys from the high-temperature oxidation in air”, J. Nucl. Mater. 465 (2015) 400–406

[22] J.H. Park, H.-G. Kim, J. Park, Y.-I. Jung, D.-J. Park, Y.-H. Koo, “High temperature steam-oxidation behavior of arc ion plated Cr coatings for accident tolerant fuel claddings”, Surf. Coatings Technol. 280 (2015) 256–259

[23] D.J. Park, H.G. Kim, Y. Il Jung, J.H. Park, J.H. Yang, Y.H. Koo, “Behavior of an improved Zr fuel cladding with oxidation resistant coating under loss-of-coolant accident conditions”, J. Nucl. Mater. 482 (2016) 75–82

[24] H. Shah, J. Romero, P. Xu, B. Maier, G. Johnson, J. Walters, et al., “Development of Surface Coatings for Enhanced Accident Tolerant Fuel”, in: Water React. Fuel Perform. Meet., Jeju Island, Korea, (2017)

[25] H.-G. Kim, I.-H. Kim, Y.-I. Jung, D.-J. Park, J.-H. Park, J.-H. Yang, et al., “Progress of Surface Modified Zr Cladding Development for ATF at KAERI”, Proceedings of Water React. Fuel Perform. Meet., Jeju Island, Korea, (2017)

[26] W. Zhong, P.A. Mouche, B.J. Heuser, “Response of Cr and Cr-Al coatings on Zircaloy-2 to high temperature steam”, Journal of Nuclear Materials 498 (2018) 137-148

[27] M. Sevecek, A. Gurgen, A. Seshadri, Y. Che, M. Wagih, B. Phillips, V. Champagne, K. Shirvan, “Development of Cr cold spray-coated fuel cladding with enhanced accident tolerance”, Nuclear Engineering and Technology, Volume 50, Issue 2, (March 2018), 229-236

[28] Y. Wang, W. Zhou, Q. Wen, X. Ruan, F. Luo, G. Bai, Y. Qing, D. Zhu, Z. Huang, Y. Zhang, T. Liu, R. Li, “Behavior of plasma sprayed Cr coatings and FeCrAl coatings on Zr fuel cladding under loss-of-coolant accident conditions”, Surface & Coatings Technology 344 (2018) 141–148

[29] J. Krejcí, J. Kabatova, F. Manoch, J. Kocí, L. Cvrcek, J. Malek, S. Krum, P. Sutta, P. Bublíkova, P. Halodova, H. K. Namburi, M. Sevecek “Development and testing of multicomponent fuel cladding with enhanced accidental performance”, Nuclear Engineering and Technology, In press (available on-line August 2019)

[30] H. Yeom, T. Dabney, G. Johnson, B. Maier, M. Lenling, K. Sridharan, “Improving deposition efficiency in cold spraying chromium coatings by powder annealing”, The International Journal of Advanced Manufacturing Technology 100 (2019) 1373–1382

[31] X. Hu, C. Dong, Q. Wang, B. Chen, H. Yang, T. Wei, R. Zhang, W. Gu, D. Chen, “High-temperature oxidation of thick Cr coating prepared by arc deposition for accident tolerant fuel claddings”, Journal of Nuclear Materials 519 (2019) 145–156

[32] B. Maier, H. Yeom, G. Johnson, T. Dabney, J. Walters, P. Xu, J. Romero, H. Shah, K. Sridharan, “Development of cold spray chromium coatings for improved accident tolerant zirconium-alloy cladding”, Journal of Nuclear Materials 519 (2019) 247–254

[33] J.C. Brachet, J. Pelchat, D. Hamon, R. Maury, P. Jacques, J.P. Mardon, “Mechanical behavior at Room Temperature and Metallurgical study of Low-Tin Zy-4 and M5™ alloys after oxidation at

1100°C and quenching", Proceedings of the Technical Committee Meeting on Fuel Behavior Under Transient and LOCA Conditions, IAEA-TECDOC-1320, Halden, Norway, (Sept 10–14, 2001), pp. 139–158

[34] L. Portier, T. Bredel, J.C. Brachet, V. Maillot, J.P. Mardon, A. Lesbros, "Influence of Long Service Exposures on the Thermal-Mechanical Behavior of Zy-4 and M5 Alloys in LOCA Conditions," J. ASTM Int. 2 (2005), JAI12468

[35] J.C. Brachet, V. Maillot, L. Portier, D. Gilbon, A. Lesbros, N. Waeckel and J.P. Mardon, "Hydrogen Content, Pre Oxidation and Cooling Scenario Influences on Post-Quench Mechanical Properties of Zy-4 and M5™ Alloys in LOCA Conditions - Relationship with the Post-Quench Microstructure", Journal of ASTM International 5 (2008) Paper ID JAI101116

[36] M. Le Saux, J.C. Brachet, V. Vandenberghe, E. Rouesne, S. Urvoy, A. Ambard, R. Chosson, "Effect of a pre-oxide on the high temperature steam oxidation of Zircaloy-4 and M5$_{Framatome}$ Alloys", Journal of Nuclear Materials 518 (2019) 386–399

[37] V. Garat, C. Ly, J.P. Mardon, L. Gerken, D. Deveney, D. Deuble, "AREVA NP M5® Cladding Benefits for Proposed US NRC RIA and LOCA Requirements", Proceedings of TopFuel 2016 Conference, Boise, ID, USA, (September 2016)

[38] A. Sawatzki, G. A. Ledoux, S. Jones, "Oxidation of Zirconium During a High Temperature Transient", Zirconium in the Nuclear Industry, ASTM STP 633, A. L. Lowe, Jr. and G. W. Parry, Eds., American Society for Testing materials, (1977) 134–149

[39] H.M. Chung and T.F. Kassner, "Embrittlement Criteria for Zircaloy Fuel Cladding Applicable to Accident Situations in Light-Water Reactors", Summary Report, NUREG/CR-1344, ANL-7948, (1980)

[40] M. Négyesi, L. Novotný, J. Kabátová, S. Linhart, V. Klouček, J. Lorinčík, V. Vrtílková, "UJP LOCA Oxidation Criteria "K" and "Oβ"", IAEA-TECDOC-CD-1709, (2013)

[41] E. A. Gulbransen, K. F. Andrew, J. Electrochem. Soc. 99 (1952) 402–406

[42] C. A. Phalnikar, E. B. Evans, W. M. Baldwin, J. Electrochem. Soc. 103 (1956) 429–438

[43] W. C. Hagel, A. U. Seybolt, J. Electrochem. Soc. 108 (1961) 1146–1152

[44] L. Cadiou, J. Paidassi, Memoires Scientifiques De La Revue De Metallurgie. 66 (1969) 217–225

[45] D. Caplan, G. I. Sproule, Oxidation of Metals. 9 (1975) 459–472

[46] K. P. Lillerud, P. Kofstad, J. Electrochem. Soc. 127 (1980) 2410–2419

[47] A. Atkinson, R. I. Taylor, Transport in Nonstoichiometric Compounds, ed. G. Simkovich and V.S. Stubican. 129 (1985) 285–295

[48] K. Taneichi, T. Narushima, Y. Iguchi, and C. Ouchi, Materials Transactions. 47 (2006) 2540–2546

[49] L. Bataillou, C. Desgranges, L. Martinelli, D. Monceau, "Modelling of the Effect of Grain Boundary Diffusion on the Oxidation of Ni-Cr Alloys at High Temperature", Corrosion Science 136 (2018) 148–160

[50] L. Royer, X. Ledoux, S. Mathieu, P. Steinmetz, "On the Oxidation and Nitridation of Chromium at 1300°C", Oxid. Met. 74 (2010) 79–92

[51] J. Ribis, A. Wu, J.-C. Brachet, F. Barcelo, and B. Arnal , "Atomic-scale interface structure of a Cr-coated Zircaloy-4 material", Journal of Materials Science 53 (2018) 9879–9895

[52] A. Wu, J. Ribis, J.-C. Brachet, E. Clouet, F. Leprêtre, E. Bordas, B. Arnal, "HRTEM and chemical study of an ion-irradiated chromium/zircaloy-4 Interface", Journal of Nuclear Materials 504 (2018) 289–299

[53] W. Xiang, S. Ying, "Reaction Diffusion in Chromium-Zircaloy-2 System" CNIC-01562 / SINRE-0096 NPIC report, (1993)

[54] J.G. Gigax, M. Kennas, H. Kim, B.R. Maier, H. Yeom, G.O. Johnson, K. Sridharan, L. Shao, "Interface reactions and mechanical properties of FeCrAl-coated Zircaloy-4", Journal of Nuclear Materials 519 (2019) 57–63

[55] E. C. Subbaraoh, S. Maiti, K. K. Srivastava, “Martensitic Transformation in Zirconia” (Review Article), Phys. Stat. Sol. (a) 21, 9 (1974)

[56] J.-C. Brachet, V. Vandenberghe, “Comments to papers of J. H. Kim et al. and M. Große et al. recently published in JNM on the hydrogen uptake of Zircaloy-4 and M5™ alloys subjected to steam oxidation in the 1100-1250°C temperature range”, Journal of Nuclear Materials 395 (2009) 169–172

[57] G. Hache, H.M. Chung, “The History of the LOCA embrittlement criteria”, Topical Meeting on LOCA Fuel Safety Criteria held in Aix-en-Provence, OECD- NEA, (2001), pp. 37–64

[58] C. Grandjean, G. Hache, “A State-Of-the-Art Review of past programmes devoted to fuel behavior under LOos-of-Coolant-Accident conditions. Part 3: Cladding oxidation. Resistance to quench and post-quench loads”, IRSN Technical Report, DPAM/SEMCA 2008-093, (2008), p.28

[59] “State-of-the-art Report Nuclear on Fuel Behaviour in Loss-of-coolant Accident (LOCA) Conditions”, OECD Report, (2009), NEA No. 6846

[60] L. Baker and L.C. Just, “Studies of metal-water reactions at high temperatures. III. Experimental and theoretical studies of the zirconium-water reaction”, ANL-6548, ML050550198, (May 1962)

[61] Atomic Energy Commission Rule-Making Hearing, Opinion of the Commission, Docket RM-50-1, (28 December, 1973)

[62] Atomic Energy Commission Rule-Making Hearing, Concluding Statement of the Regulatory, Staff, Docket RM-50-1, (16 April, 1973)

[63] Acceptance Criteria for Emergency Core Cooling Systems for Light-Water Nuclear Power Reactors, U.S. Code of Federal Regulations, Title 10, Part 50, Section 46 (1974)

[64] J. Debuigne, “Contribution to Study of Zirconium Oxidation and oxygen Diffusion into the Oxide and the Metal”, PhD Thesis, Faculté des sciences de Paris – in French (1966)

[65] X. Ma, C. Toffolon-Masclet, T. Guilbert, D. Hamon, J.C. Brachet, “Oxidation kinetics and oxygen diffusion in low-tin Zircaloy-4 up to 1523 K”, Journal of Nuclear Materials 377 (2008) 359–369

[66] C. Corvalan-Moya, C. Desgranges, C. Toffolon-Masclet, C. Servant, J.C. Brachet, “Numerical modelling of oxygen diffusion in the wall thickness of low-tin zircaloy-4 fuel cladding tube during high temperature (1100°C-1250°C) steam oxidation”, Journal of Nuclear Materials 400 (2010) 196–204

[67] A. V. Berdyshev, M. S. Veshchunov, Proceedings of Nuclear Safety Institute (IBRAE-RAS), Vol. 1, pp. 6–14 (2010)

[68] H. Xiaoqiang, Y. Hongxing, J. Guangming. proceedings of 2011 Water Reactor fuel Performance Meeting Conference Proceeding T3-040, Chengdu, China, (Sept 11–14, 2011)

[69] B. Mazères, C. Desgranges, C. Toffolon-Masclet, D. Monceau, “Contribution to Modelling of Hydrogen Effect on Oxygen Diffusion in Zy-4 Alloy During High Temperature Steam Oxidation”, Oxid. Met. 79 (2013) 121–133

[70] D.-B. Wei, P.-Z. Zhang, Z.-J. Yao, W.-P. Liang, Q. Miao, Z. Xu, “Oxidation of double-glow plasma chromizing coating on TC4 titanium alloys”, Corrosion Science 66 (2013) 43–50

[71] X. Han, J. Xue, S. Peng, H. Zhang, “An interesting oxidation phenomenon of Cr coatings on Zry-4 substrates in high temperature steam environment”, Corrosion Science 156 (2019) 117–124

[72] N. Chaari, J. Bischoff, Ch. Delafoy, P. Barberis, K. Nimishakavi “The behavior of Cr-coated Zirconium alloy cladding tubes at high temperatures”, 19th International ASTM Symposium on Zr in the Nuclear Industry, May 20-23, 2019, Manchester, UK, to be published in ASTM-STP

[73] N. Dupin, I. Ansara, C. Servant, C. Toffolon, C. Lemaignan, J.C. Brachet, “A Thermodynamic Database for Zirconium Alloys”, Journal of Nuclear Materials 275 (1999) 287–295

[74] P. Lafaye, “Développement d’outils de modélisation thermodynamique pour la prédiction de l’état métallurgique d’alliages à base de zirconium”, PhD Thesis, Paris-Est University (2017), *in French*

[75] D. Gosset, M. Le Saux, “In-situ X-ray diffraction analysis of zirconia layer formed on zirconium alloys oxidized at high temperature”, Journal of Nuclear Materials 458 (2015) 245–252

[76] H. Yeom, B. Maier, G. Johnson, T. Dabney, M. Lenling, K. Sridharan, “High temperature oxidation and microstructural evolution of cold spray chromium coatings on Zircaloy-4 in steam environments”, Journal of Nuclear Materials 526 (2019) 151737

FIGURE CAPTIONS:

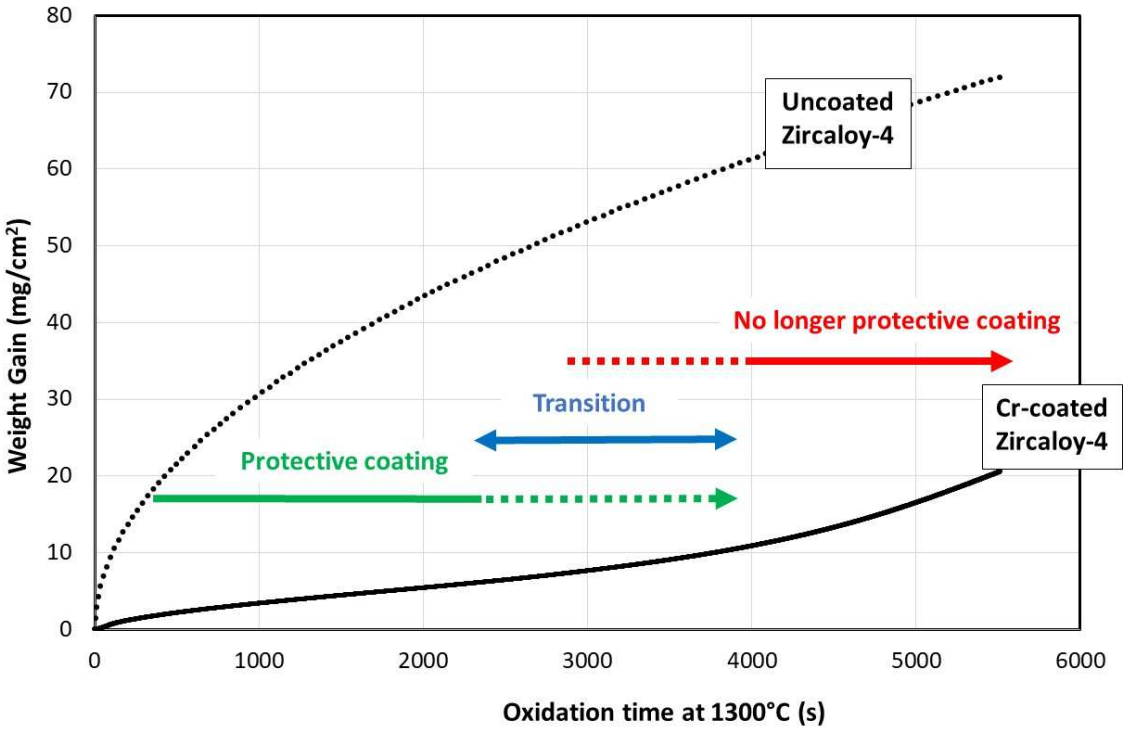

Figure 1 - Weight gain evolution measured by TGA experiments carried out in helium-oxygen mixture at 1300°C on the first generation of Cr-coated Zircaloy-4 (sheet sample geometry) compared to the weight gain evolution of uncoated Zircaloy-4

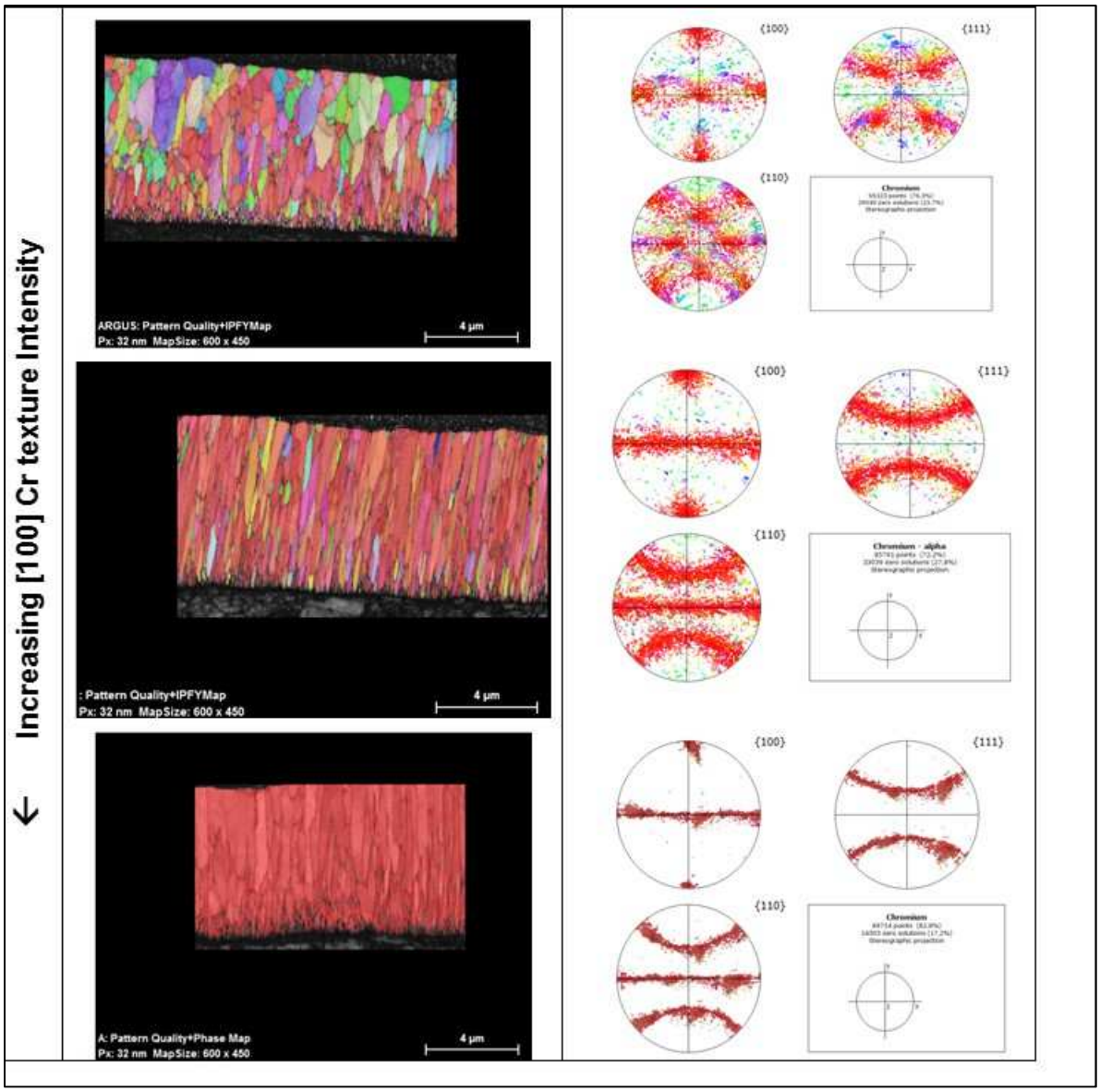

Figure 2 - Typical EBSD orientation maps and associated stereographic pole figures of the first generation 5-10µm-thick Cr-coated Zircaloy-4 (sheet substrate), obtained with different PVD deposition parameters

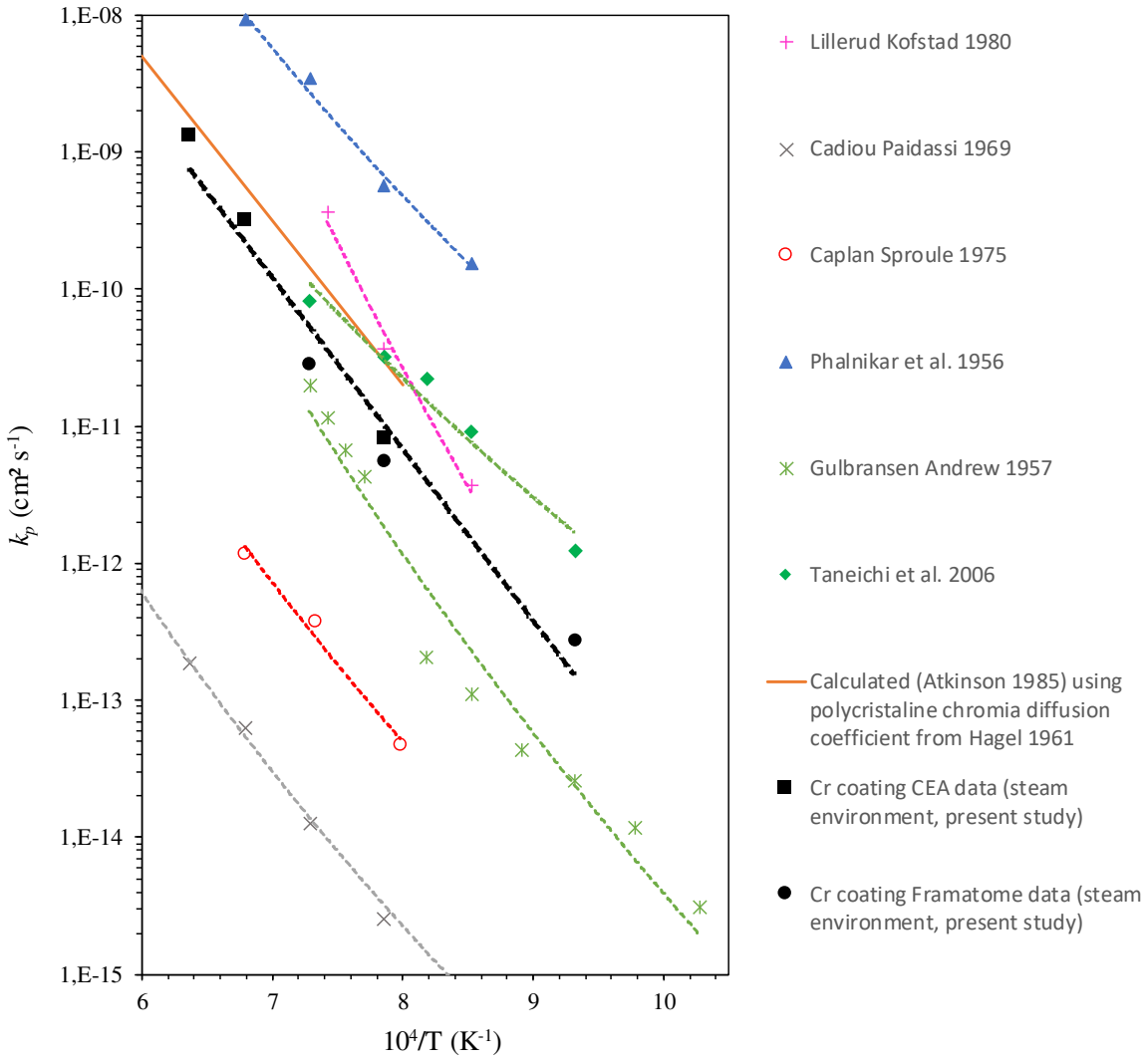

Figure 3 - Arrhenius plot of the rate constant of the parabolic law describing the growth of Cr_2O_3 upon HT oxidation, reported in the literature for pure chromium (oxidized in air or oxygen) [41]-[48] (replotted from [49]) and from the present study for Cr-coatings (steam oxidation, short oxidation times)

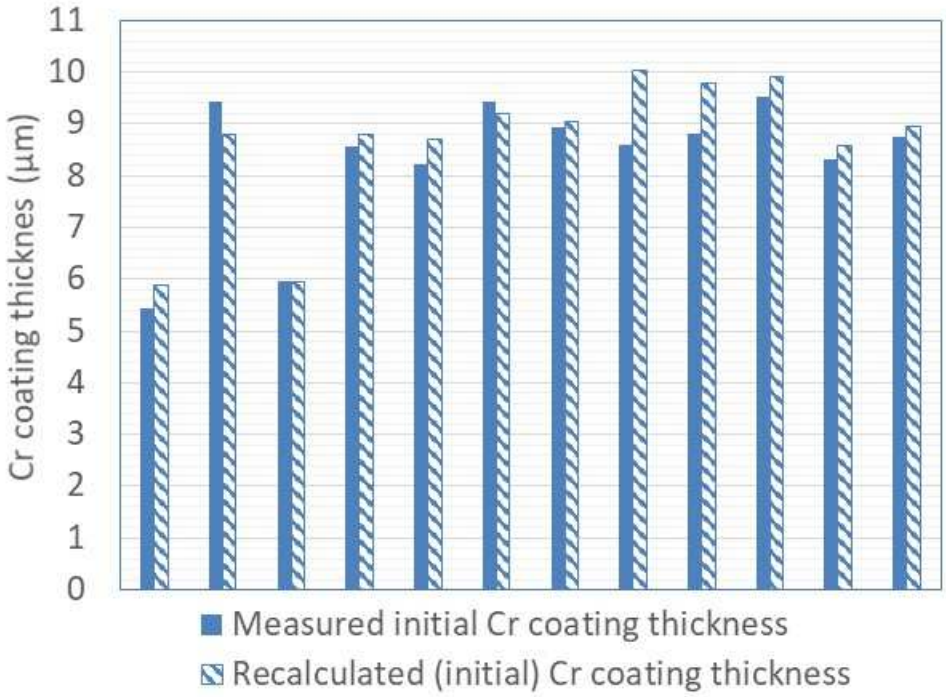

Figure 4 - Comparison between measured thicknesses of the as-received Cr-coating and (post-HT oxidation) recalculated thicknesses, for several first generation 5-10µm-thick Cr coated Zircaloy-4 samples that have been subjected to steam oxidation up to 1500s at 1200°C.

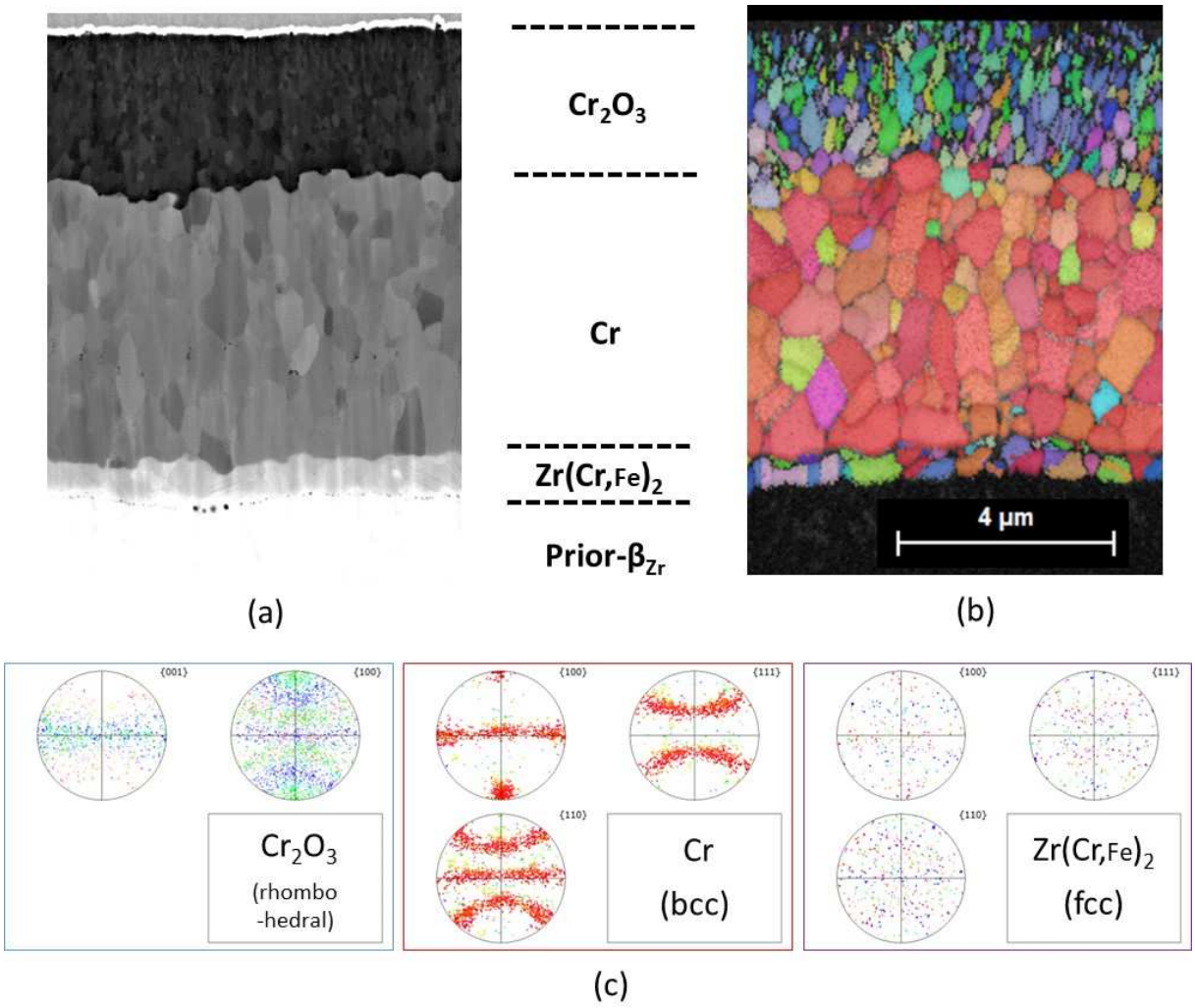

Figure 5 - PQ typical microstructure of a first generation 5-10µm-thick Cr-coated Zircaloy-4 sample after steam oxidation for 300s at 1200°C (protective coating): (a) SEM micrograph (Back-Scatter Electron mode, BSE), (b) EBSD crystallographic orientation map, (c) corresponding pole figures

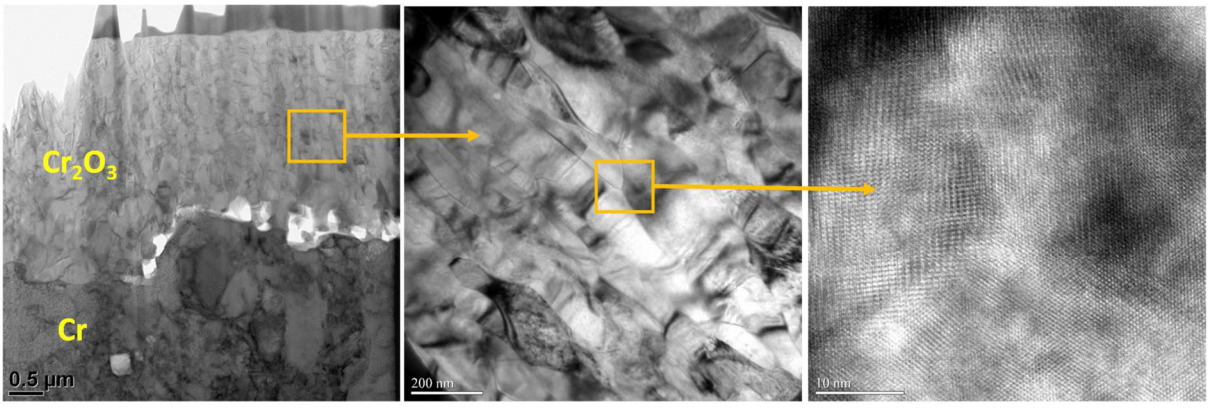

(a) Overall view of Cr_2O_3/Cr outer scales (low magnification)

(b) Intermediate magnification - Cr_2O_3 scale

(c) HRTEM examination of a triple grain boundary - Cr_2O_3 scale

Figure 6 **-** Conventional and HRTEM micrographs of the outer scales formed upon HT steam oxidation on Cr-coated Zircaloy-4 sheet sample from the first generation

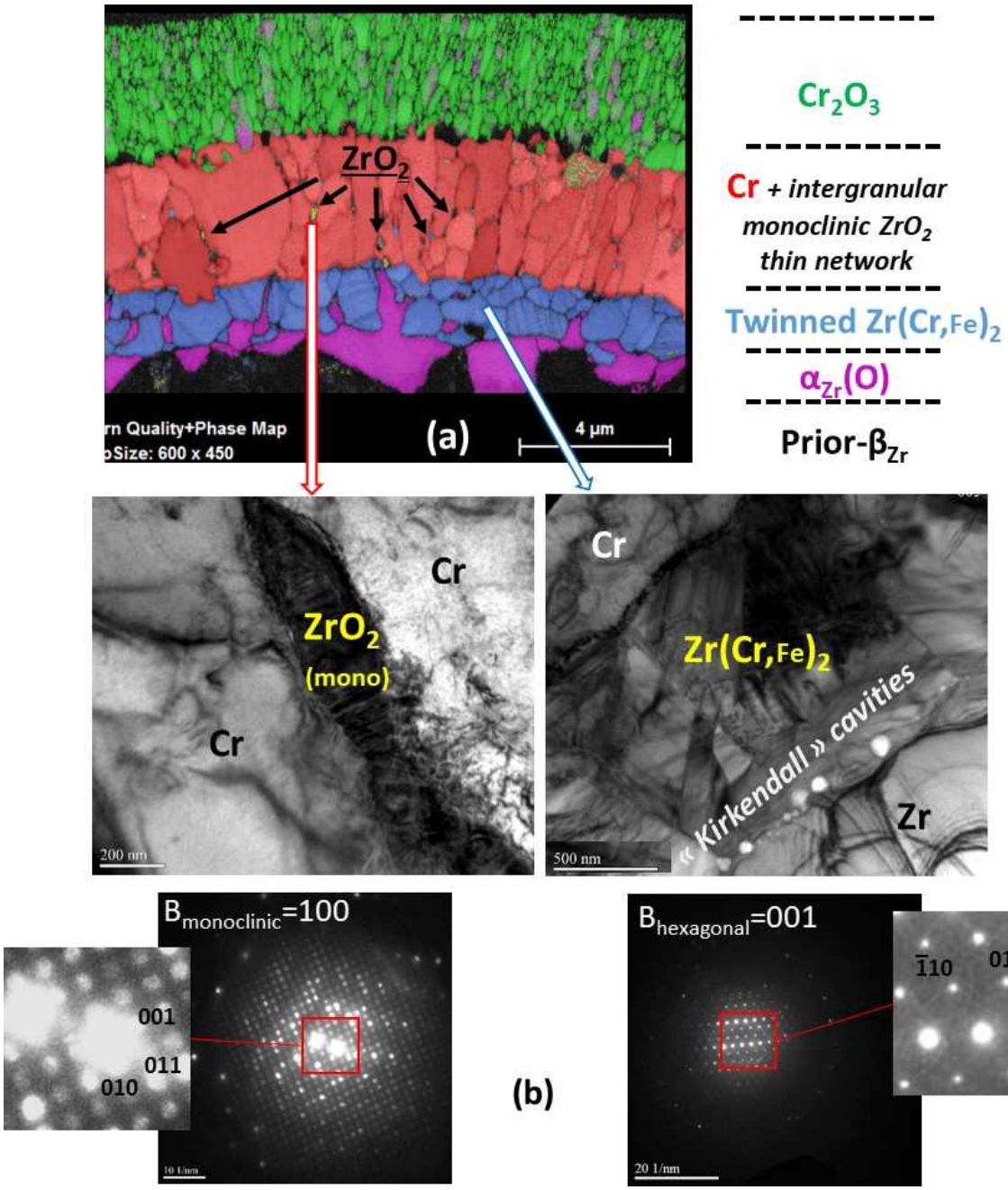

Figure 7 - PQ typical microstructure of a 5-10µm-thick Cr-coated Zircaloy-4 sheet sample from the first generation after steam oxidation for 1400s at 1200°C (transition stage):
(a) SEM-EBSD phase map,
(b) TEM micrographs and associated electron diffraction patterns of a metallic chromium grain boundary decorated with an intergranular ZrO_2 layer (left) and of the Zr/Cr interface with $Zr(Cr,Fe)_2$ intermetallic phase (right)

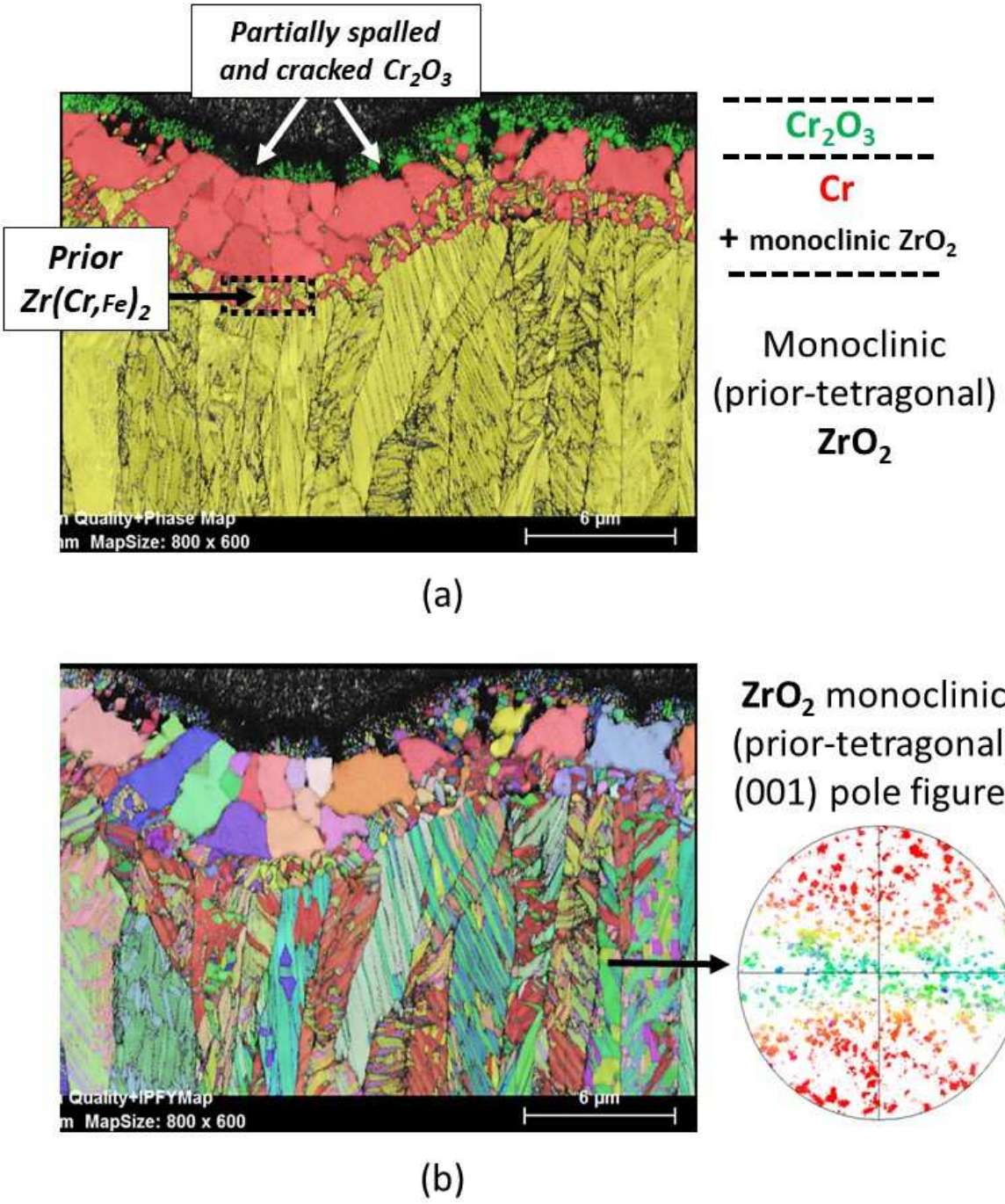

Figure 8 - PQ typical microstructure of a thin (5µm-thick) Cr-coated Zircaloy-4 sheet sample from the first generation after steam oxidation for more than 1400s at 1200°C (no-longer protective coating): (a) EBSD phase-map, (b) EBSD crystallographic orientation map and corresponding (001) pole figure of monoclinic ZrO_2

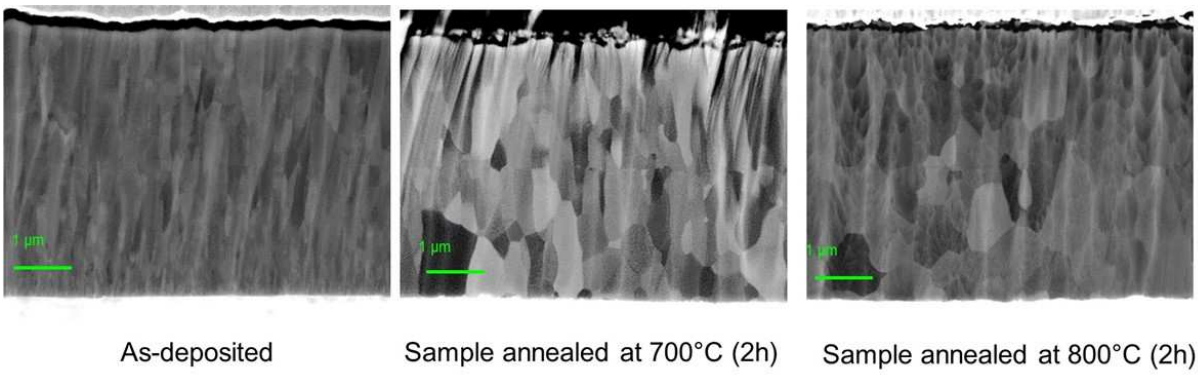

Figure 9 - SEM-BSE micrographs of the outer chromium coating as-deposited and annealed at 700 and 800°C for two hours

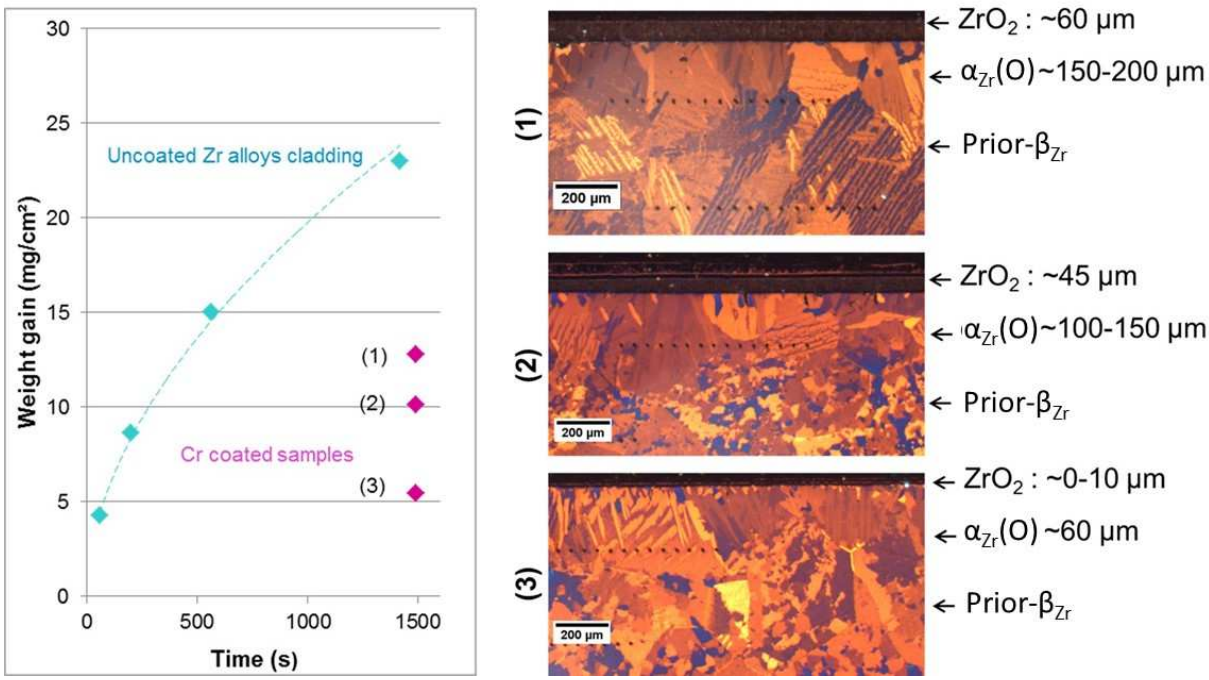

Figure 10 - Comparison of the weight gains of uncoated and 6-8µm-thick Cr-coated Zr alloys claddings after steam oxidation at 1200°C and corresponding PQ optical micrographs (polarized light): (1) as-deposited, (2) pre-annealed for 2h at 700°C, (3) pre-annealed for 2h at 800°C
(the residual outer oxidized Cr-coating scale is too thin to be observed at such magnification and thus has not been pointed out on the optical micrographs)

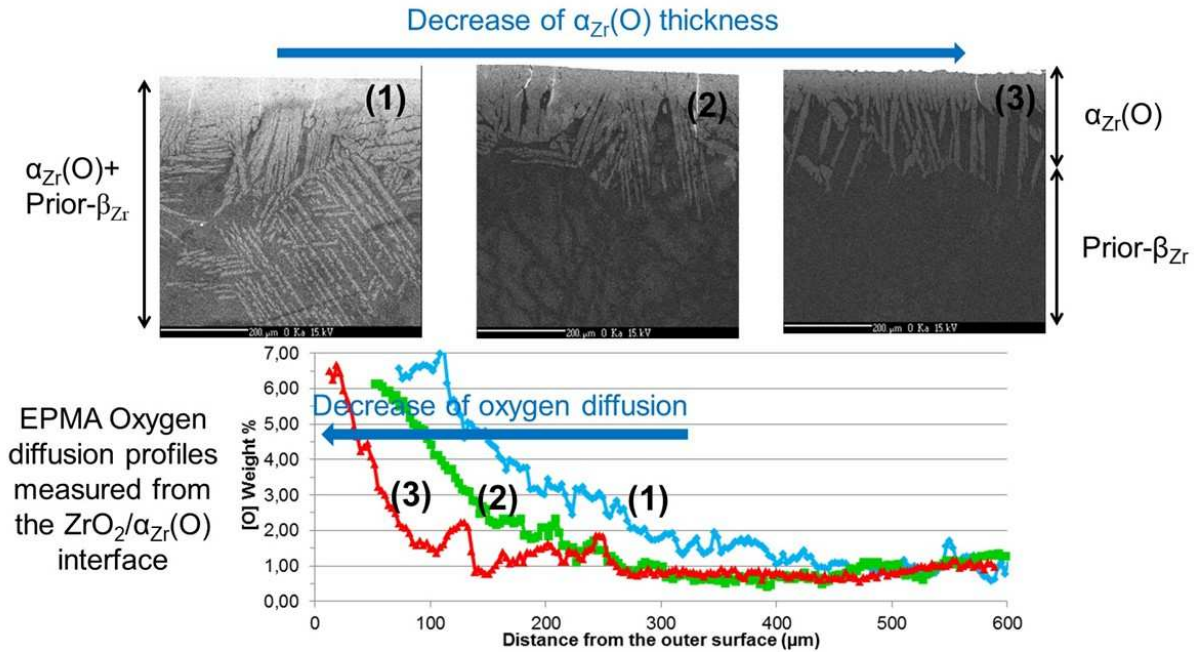

Figure 11 - PQ SEM-BSE micrographs and oxygen concentration profiles (from EPMA measurements) within the inner prior-β_{Zr} layer of uncoated and 6-8µm-thick Cr-coated Zr1Nb(O) alloy steam oxidized for 1500s at 1200°C: (1) as-deposited, (2) pre-annealed 2h at 700°C, (3) pre-annealed 2h at 800°C materials

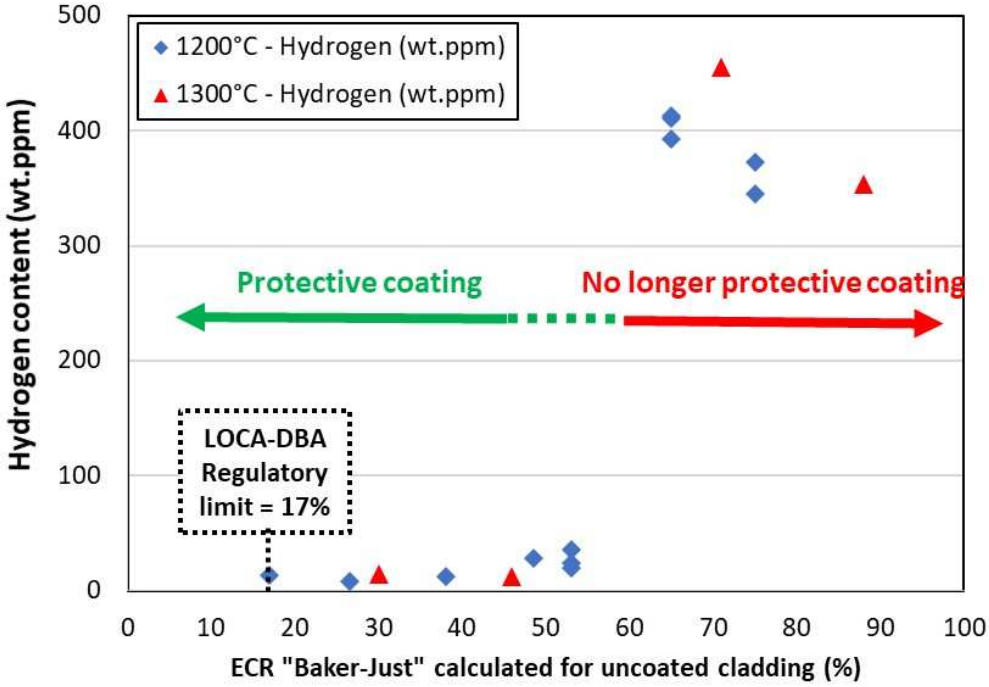

(a)

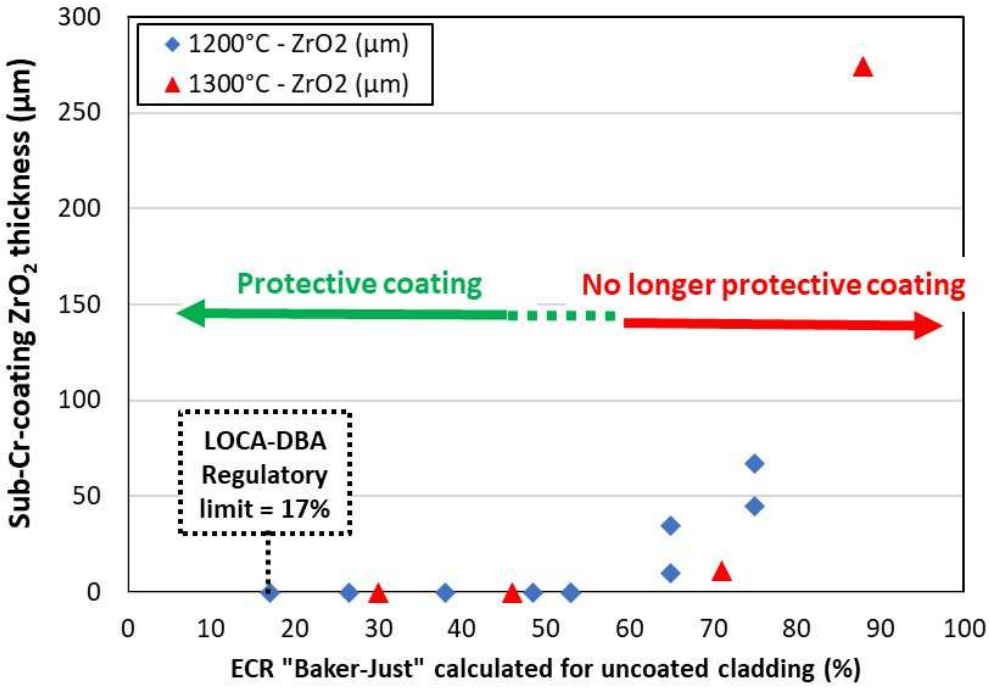

(b)

Figure 12 - Evolution of (a) the hydrogen content and (b) the zirconia layer (beneath the residual Cr-coating) thickness, as a function of the calculated ECR-BJ upon steam oxidation at both 1200°C and 1300°C for 12-17µm-thick Cr-coated $M5_{Framatome}$ claddings

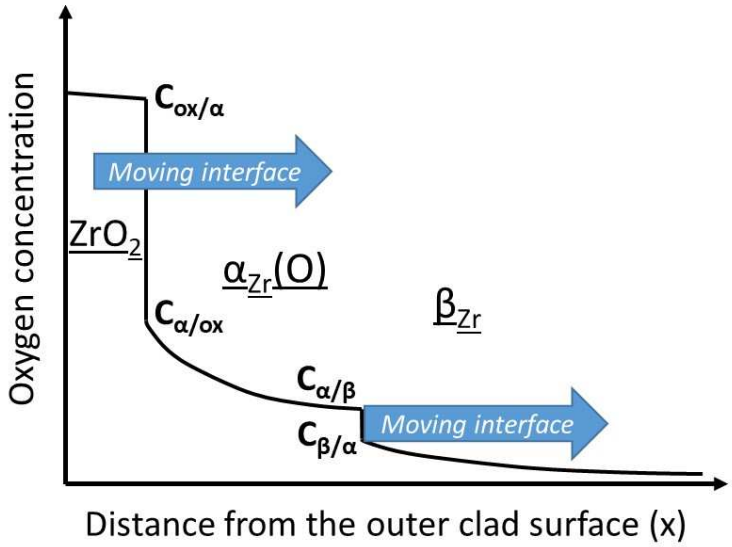

Figure 13 - The different layers formed upon HT oxidation in uncoated reference zirconium-based (Zircaloy-type) alloys and associated oxygen concentration profile through the clad wall thickness

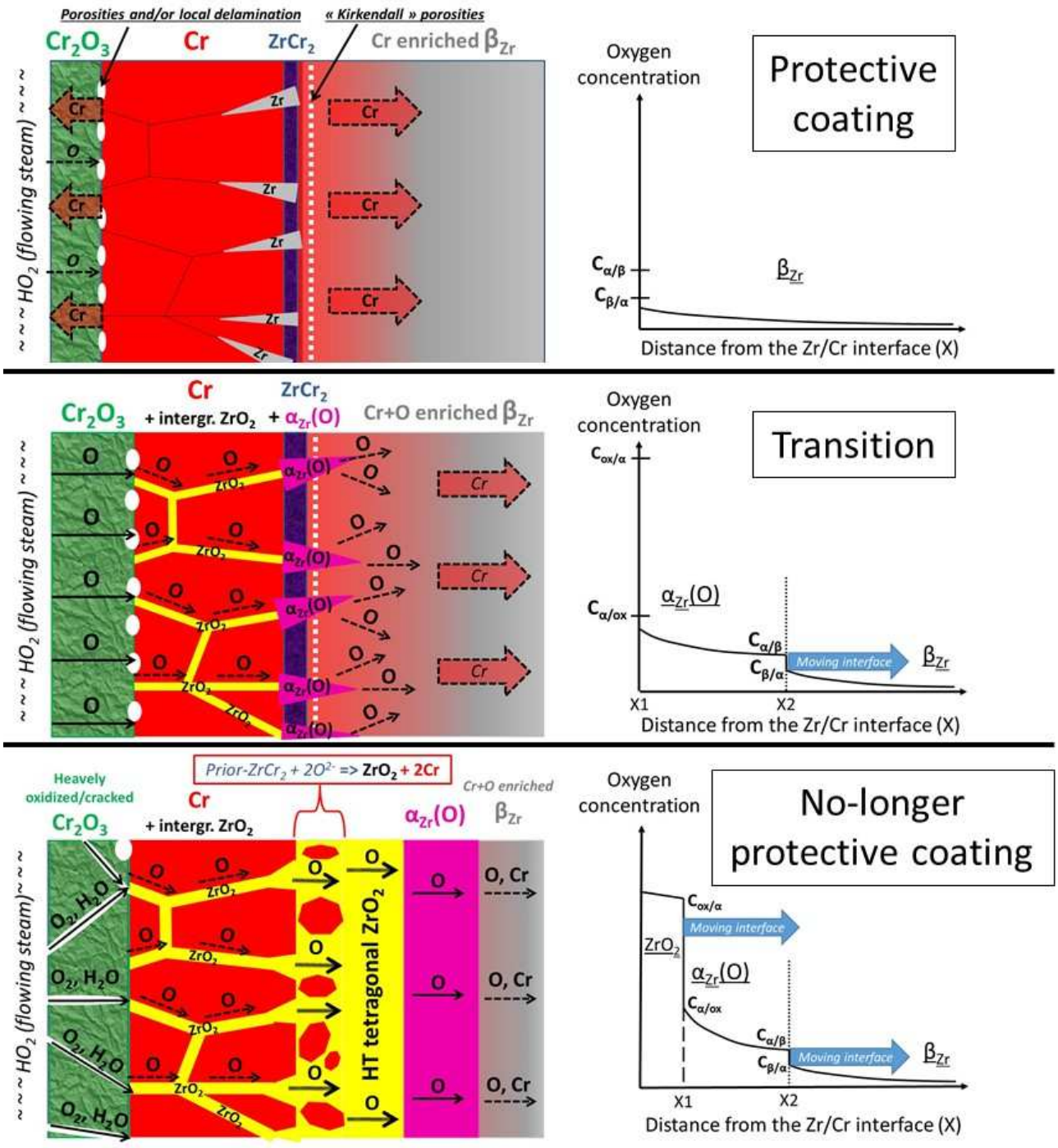

Figure 14 - Schematic overview of the HT steam oxidation process of Cr-coated zirconium-based (Zircaloy-type) alloys

(this figure is only qualitative and for schematic purpose; thus, it does not reproduce the actual thicknesses of the different layers, which are related to the initial Cr-coating thickness and microstructure, that may differ from one sample to another)

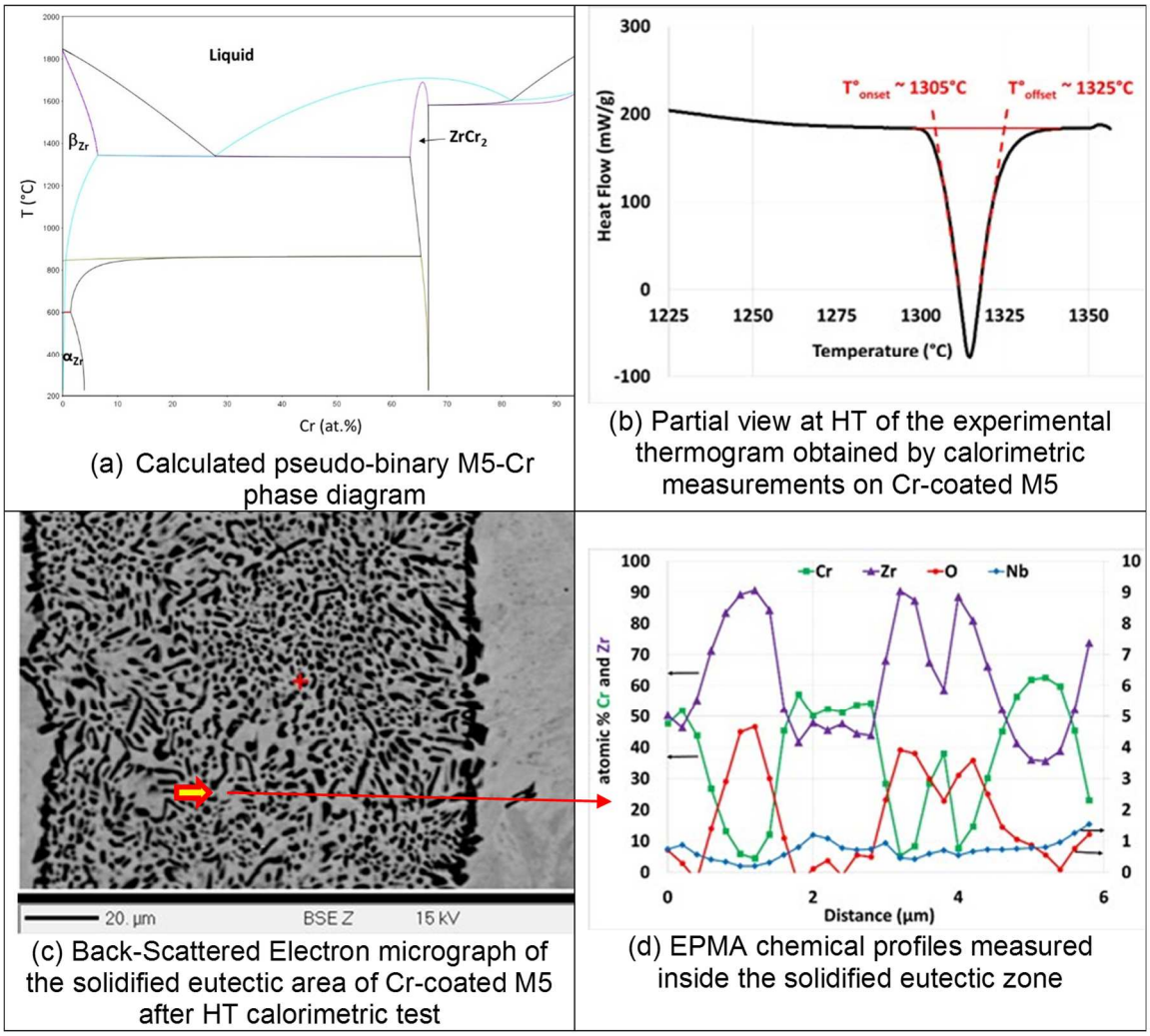

(a) Calculated pseudo-binary M5-Cr phase diagram

(b) Partial view at HT of the experimental thermogram obtained by calorimetric measurements on Cr-coated M5

(c) Back-Scattered Electron micrograph of the solidified eutectic area of Cr-coated M5 after HT calorimetric test

(d) EPMA chemical profiles measured inside the solidified eutectic zone

Figure 15 - Calculated pseudo-binary $M5_{Framatome}$-Cr phase diagram, partial thermogram from calorimetric measurements, associated microstructures and chemical profiles, underlying the M5-Cr eutectic reaction at temperatures above 1300°C

Figure 16 - Typical PQ aspect of a 12-15µm thick Cr-coated $M5_{Framatome}$ cladding sample after HT oxidation for 100s at 1400°C followed by direct water quenching

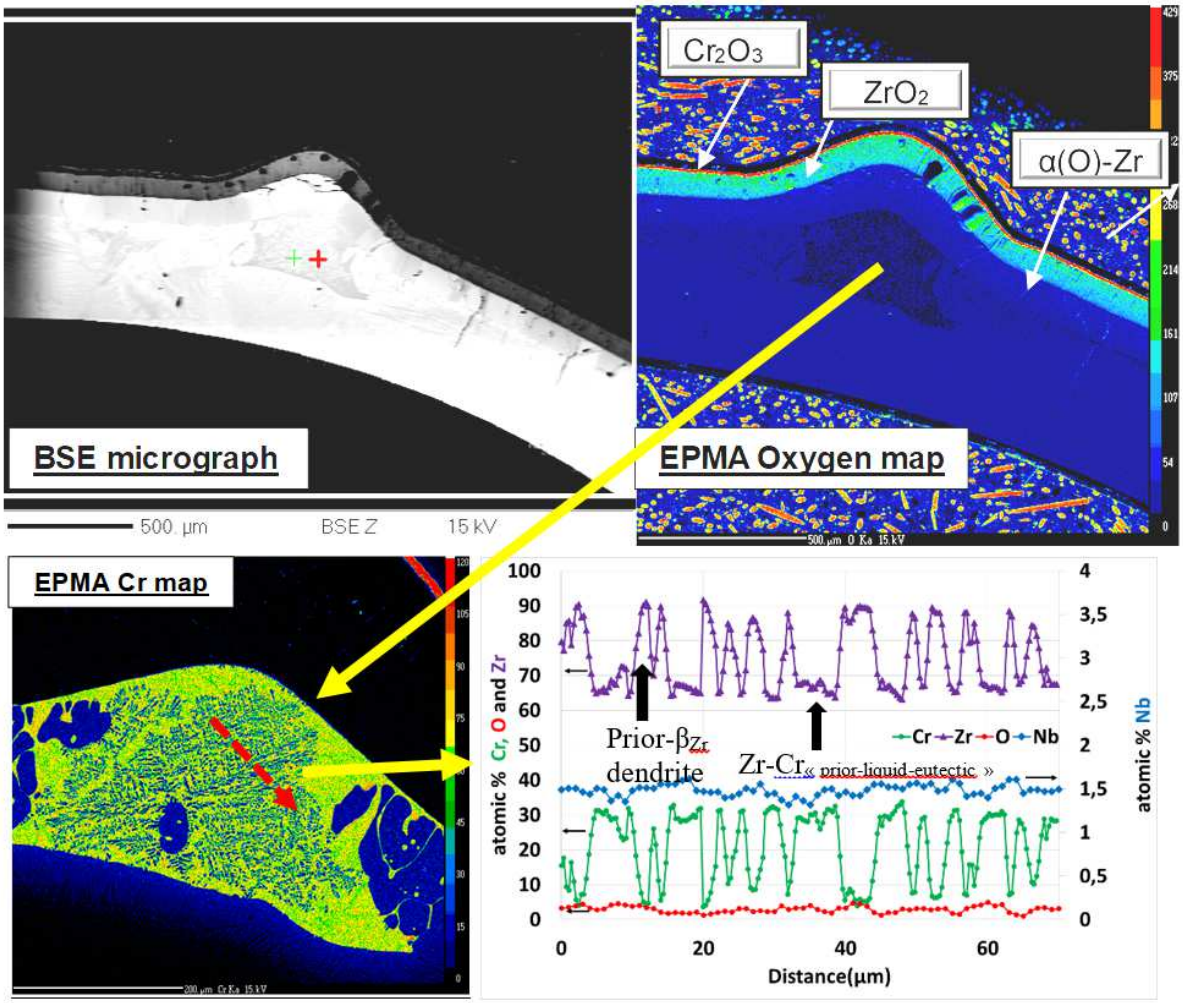

Figure 17 - EPMA chemical element mapping and quantitative profiles obtained at the vicinity of a protruding blister in a Cr-coated $M5_{Framatome}$ cladding segment one-sided steam oxidized for 100s at ~1400-1450°C and water quenched down to room temperature

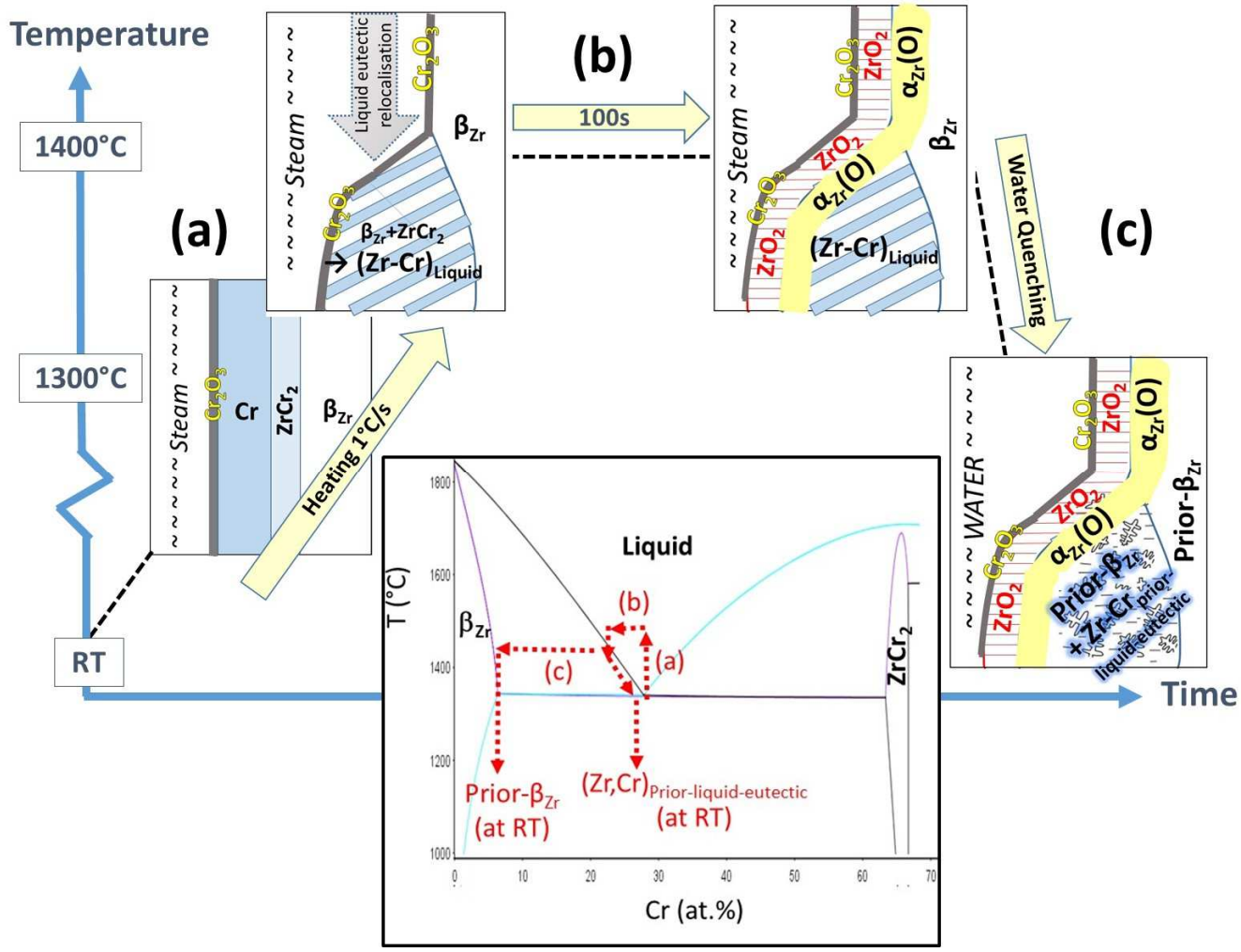

Figure 18 - Phenomenological description of the mechanisms of HT oxidation of Cr-coated $M5_{Framatome}$ at temperatures above 1300°C, involving eutectic formation and re-solidification; corresponding calculated pseudo-binary $M5_{Framatome}$-Cr phase diagram

Oxidation temperature (°C)	Oxidation time (s)	ECR-BJ (%)	Hydrogen content (wt.ppm)	ZrO_2 thickness (µm)
1200°C	600	17	14	0
	1500	26,5	8	0
	3000	38	13	0
	5000	48,5	28	0
	6000	53	20	~ 0
			24	
			35	
	9000	65	394	10 - 35
			411	
			414	
	12000	75	345	45
			374	
1300°C	920	30	15	0
	2200	46	13	0
	5300	71	456	11
	9200	88	353	274

Table 1 – Oxidation conditions, corresponding ECR-BJ values and associated PQ hydrogen contents and sub-coating zirconia thicknesses measured for 12-15µm-thick Cr-coated $M5_{Framatome}$ after one-sided steam oxidation at 1200 and 1300°C